12-2022

Establishing the efficacy of non-cellular components of adipose-derived stromal vascular fraction in promoting angiogenesis.

Daniel Benson
University of Louisville

ESTABLISHING THE EFFICACY OF NON-CELLULAR COMPONENTS OF ADIPOSE-DERIVED STROMAL VASCULAR FRACTION IN PROMOTING ANGIOGENESIS

By

Daniel Ray Benson II

B.S., University of Louisville, 2021

A Thesis

Submitted to the Faculty of the

J.B. Speed School of Engineering of the University of Louisville

In Partial Fulfilment of the Requirements

For the Degree of

Master of Engineering

In Bioengineering

Department of Bioengineering

University of Louisville

Louisville, KY.

December 2022

ESTABLISHING THE EFFICACY OF NON-CELLULAR COMPONENTS OF ADIPOSE-DERIVED STROMAL VASCULAR FRACTION IN PROMOTING ANGIOGENESIS

By

Daniel Ray Benson II

B.S., University of Louisville, 2021

A Thesis Approved on

December 5, 2022

By the following Thesis Committee:

_____

Dr. Patricia Sara Arauz Soucy, Thesis Chair

_____

Dr. Amanda Jo LeBlanc, Thesis Co-Chair

_____

Dr. Martin G. O'Toole, Committee member

DEDICATION

I would like to dedicate this thesis to those who breathe life into their ideas. This thesis is for people who first have a dream and imagine what they want to do in the world, and then bring it to fruition. I only dreamed of doing something like this when I was younger until I woke up one day and was doing it. This is for the people who manifest life into their imagination and take an idea into reality. Create whatever you see fit for the world and its needs.

ACKNOWLEDGEMENTS

I would like to thank Dr. Amanda Jo LeBlanc for giving me such a great opportunity with this project and the creative freedom to drive it the way I was inspired. I would also like to thank my previous mentors Dr. Anne K. Perl and Dr. William J. Zacharias for fostering my passion for research and preparing me to take on this project. My professors and mentors Dr. Jill Steinbach-Rankins and Dr. Patricia Sara Arauz Soucy also deserve much appreciation and thanks for their part in mentoring me throughout my studies at UofL and pushing me in my curriculum and projects to learn as much as I can.

I also want to acknowledge my former lab-mates and friends Jenna Green, Andrea Toth, Jason Beare, and Dr. Gabrielle Brown for teaching me all the hands-on skills I know. I couldn't have finished this project without the support of my friends, family, and the friends who are my family.

ABSTRACT

ESTABLISHING THE EFFICACY OF NON-CELLULAR COMPONENTS OF ADIPOSE-DERIVED STROMAL VASCULAR FRACTION IN PROMOTING ANGIOGENESIS

Daniel Ray Benson II

December 2022

Microvascular disease is hallmarked by pathophysiological conditions such as endothelial senescence, intimal thickening which impairs vasodilation, and regression of the capillary beds causing tissue ischemia in the myocardium or in peripheral vascular networks. Adipose-derived stromal vascular fraction (SVF) has previously demonstrated the ability to revascularize tissue. Increasing evidence shows that regenerative cells elicit their therapeutic benefit by paracrine mechanisms, leaving open extracellular vesicles (EVs) as a potential crux of the cell therapy paradigm. To test this idea, three types of gelatin methacrylate hydrogels were employed: SVF gels, EV gels derived from SVF, and blank control gels, which were used *in-vitro* and *in-vivo* to evaluate the effect of cell versus cell-free therapies for revascularizing tissues. Fischer 344 Green Fluorescent Protein positive (GFP+) male and female 6-month-old rats were used as donors for SVF, which was harvested by enzymatic digestion, centrifugation, and filtration steps. Cells were placed directly into gelatin methacrylate (GelMA) hydrogels. EVs were harvested from SVF tissue culture supernatants prior to being loaded in gel constructs. EVs were

isolated by ultracentrifugation at 100,000g from cell culture supernatants and detected by spectral flow cytometry (Cytek Aurora) utilizing violet laser side scatter height and characterized by expression of CD9 and CD63 markers. This detection method was also used to estimate the number of particles from a known number of SVF cells. Degradation studies of unloaded GelMA hydrogels were performed using six or eight percent (w/v) concentration over 60 days in PBS. Hydrogels were further characterized by viability assays of the SVF gels to ensure the gel synthesis process, specifically UV exposure, was not cytotoxic to SVF. EV hydrogels were also characterized by their release over 7 days. A plug-in-field assay was used to determine the vasculogenic efficacy of the groups *in vitro* by staining the constructs with Griffonia Simplicifolia Lectin I (GS1+) and DAPI after seven and fourteen days in culture; plugs were explanted, and images were analyzed for cellular presence and expression of GS1 and αSMA markers. Finally, experimental and control gels were implanted bilaterally into the dorsal subcutaneous space of Rag1 mice for 14 days. Prior to explant, dextran tetramethylrhodamine was infused, gels were explanted and stained for cell markers, and imaged via confocal microscopy. Analysis of images acquired from *in vivo* experiments were compared for angiogenic metrics such as vascular density, indicated by the dextran infusion.

TABLE OF CONTENTS

LIST OF FIGURES

INTRODUCTION

Vascular disease is a common pathology seen with aging. However, emerging research shows vascular disease does not present the same between the sexes [1]. Specifically, men present with more narrow, and plaque occluded larger arteries, while women present their cardiovascular dysfunction within the microcirculation, including pathologies such as intimal thickening at the arteriole level, endothelial senescence, hyper-constriction, and regression of the microcapillaries in the coronary and peripheral vasculature [2, 3]. Current pharmacological therapies remedy smooth muscle of the large artery occlusion characteristic in men but do not directly combat the pathology seen more often in women [4].

Endothelial networks are crucial for cellular and tissue function throughout the body. These networks help provide oxygen and nutrients to specific tissues required for survival and promote cellular health by removing waste products from the capillary beds [5]. During normal physiological remodeling, hypoxia causes existing vessels to break down their basement membrane and allows for existing endothelial cells to proliferate into the newly vacant space. As proliferation continues budding, as well as elongation, of the neo-vessel structure occurs to termination or conjunction with another capillary in a process called angiogenesis [6]. However, certain pathologies and risk factors can lead to endothelial cell dysfunction, resulting in tissue ischemia due to lack of adequate blood supply. One of the most common causes of endothelial dysfunction is aging [5] because of the telomere shortening process seen in DNA replication that is repeated more

throughout someone's lifespan [5]. However, the dysfunction seen in vascular diseases has proved to present differently between men and women [1]. Men typically express vascular disease symptoms that include narrowing of the larger arteries and/or plaque buildup in vascular smooth muscle networks; however, women present with hyper constriction of arterioles and regression of endothelial capillary networks that are associated with the microcirculation [2]. Both vascular diseases have the same result of tissue ischemia, but the pharmacologic agents prescribed to both groups are aimed at targeting smooth muscle cells of the larger arteries to induce vasodilatation and restore blood supply, but this only alleviates the source problem in men and does not target the micro-vessel dysfunction seen more in women, termed microvascular disease (MVD) [4].

The need to stimulate tissue morphogenesis of capillary networks suggest cell therapies may be a useful solution for stimulating angiogenesis [7]. While many stem cell sources such as bone marrow mesenchymal stem cell [8-13], embryonic stem cells, induced pluripotent stem cells, adipose mesenchymal stem cells, and birth-derived tissues such as the umbilical cord, amnion, and placenta [14-16] have all displayed the ability to promote endothelial cell function [7]. The stromal cell population of adipose tissue (SVF), however, offers benefits not possessed by other sources. These benefits include a heterogeneous cell population used for therapy made up of endothelial cells, macrophages, pericytes, and various stem cell populations such as mesenchymal stem cells [7, 17], in addition to a higher concentration of stromal cell populations than bone marrow [18], and this cell source is advantageous as a potential therapy clinically because of its relatively easier harvest method being liposuction from donors [19].

Increasing evidence from cell therapy studies suggest that stem cells may elicit their therapeutic benefit along two axes: directed differentiation and paracrine effects [20-22]. Directed differentiation is the notion that the stem cells themselves incorporate into the host vasculature and differentiate into the cells needed to support the growing endothelial networks. However, emerging evidence suggest that the secretome of the various cell population, in the form of extracellular vesicles, is perhaps just as important for endothelial network changes [20, 23-25]. Moreover, it may not be as important for the cells themselves to incorporate into the tissue and directly elicit changes, but, rather, provide the necessary environmental cues to existing host cells to initiate alterations in tissue morphology [26, 27].

Adipose derived SVF has previously demonstrated the ability to revascularize injured tissue [28]. In addition to its angiogenic capacity, the cell population has also shown the ability to restore vasodilatory function in the tertiary coronary branches of rats with advanced age following tail vein injection in rats [29]. However, the therapeutic effect of the cell population's sectretome in the form of extracellular vesicles (EVs) has yet to be directly tested against the cells themselves. Mass spectrometry data of both SVF and adipose derived stem cell culture media has been shown to contain different proteins that have pro-oxidant and anti-oxidant effects which can improve mitochondrial function in coronary microvascular disease by improving levels of reactive oxygen species and reactive nitrogen species [30]. The secretome of cells containing viable agents for improving vascular health suggest EVs may be a therapeutic option worth exploring. This type of cell-free therapy would have great implications due to a lower risk of rejection by the immune system from allogeneic sources and could potentially serve a larger patient

population [7]. Extracellular vesicles have previously shown therapeutic benefits in GelMA wound models as well using exosomes derived from human umbilical vein endothelial cells [31] by accelerating wound closure, limiting wound length at the end of the study, and displaying higher vessel density and vessel formation than GelMA alone.

In this project, gelatin methacrylate (GelMA) hydrogels were employed to encapsulate either adipose-derived SVF or their derived EVs. This tissue engineered design would aim to provide cellular or non-cellular therapeutics to the public suffering from microvascular disease. As previously discussed, women suffer from this condition more often than men, and current treatments do not directly combat the need for microvascular networks in the myocardium or peripheral vasculature. This product would help close the social healthcare gap between treatments given to patients suffering from microvascular disease and treatments for large artery disease globally. The use of non-cellular therapeutics would have global implications as well due to the lower risk of immune rejection of donor cells, and the ability to harvest EV therapeutics from ongoing/passaging cultures that could potentially allow for more therapeutics to be generated.

Gels were characterized by their degradation, biocompatibility, and release of EVs, while also being assessed in *in-vitro* and *in-vivo* for their vasculogenic potential. GelMA was selected as the biomaterial because of its tunable mechanical properties [32-34], high degree of biocompatibility, and ability to be dual cross-linked [35] ensuring encapsulation of nanosized EVs [31]. **SVF hydrogels are expected to display the highest potential for vascularization based on their ability to differentiate into structures needed for blood vessels while also paracrine signaling from within the**

gel; SVF derived EV gels are expected to display potential for angiogenesis, but its therapeutic benefit may fall short of SVF gels while performing better than control gels.

METHODS

Animal Use and Care:

All animals used in this study were approved by Institutional Animal Care and Use Committee at the University of Louisville and guidelines set by the NIH *Guide for the Care and Use of Laboratory Animals* [36]. Animals had free access to food and water as well as 12-hour light and dark cycles.

SVF Isolation:

SVF samples used for therapies were collected from green fluorescent protein positive (GFP+) Fisher 344 rats as previously described [29]. SVF was harvested from male and female rat populations by isolating the ovarian fat pads and fat along fallopian tubes of females, and epididymal fat proximal to the vas deferens in males under 5% Isoflurane, and animals were euthanized before harvest via cardiac removal. Fat isolate was processed with mechanical disruption of the tissue using scissors, then was placed in a tube containing a 0.22 μm filtered solution of 0.75 mg/mL type I collagenase (vitacyte 011-1030), 1.0 mg/mL deoxyribonuclease-1 (Sigma DN25-1G), and 0.1% Bovine Serum Albumin (Sigma A6003) in HBSS (Gibco 14025-076). This mixture was allowed to homogenize in the Enviro-gene (Scientific Industries, Inc. model no. SI-1200) for 35 minutes at 37.5˚C. The tissue homogenate was centrifuged, and the adipocytes were aspirated off and the resuspended solution was passed through a 100 μm filter followed by a 20 μm filter to

remove tissue aggregates. Final cell concentration was determined using a hemocytometer (VWR Scientific 1517O-173)/Trypan Blue (Sigma T8154) stain.

SVF Cell Culture:

In order to determine EVs released from SVF, cells were plated at a concentration of ~25,000 cell/cm^2 on T-182 flask (fisherbrand FB0129939) and cultured in DMEM (Thermofisher 11885076), 10% fetal bovine serum (RND S11150), and 1% penicillin/streptomycin (Fisher 15-140-148), which was filtered through a 0.22 µm PES filter (Corning, 431161). Prior to plating, flasks were coated >20 minutes in 1% gelatin (Sigma G1890) in 1X DPBS at 37ºC and washed with 1X DPBS (Corning 21-031-CV) before the cell solution was added. 25mL media changes were collected 96 hours after 80-100% confluency was observed between all the flasks. Cells were lifted with 0.25% Trypsin-EDTA (Sigma T3924) after a 10-minute incubation where the reaction was quenched with media. The number of cells from each flask upon media collection was quantified using a hemocytometer (VWR Scientific 1517O-173)/Trypan Blue (Sigma T8154) stain.

EV Isolation by Ultracentrifugation:

EVs were diluted in sterile 1X PBS (Gibco 10010-031) and isolated by ultracentrifugation (Beckman Coulter Optima LE-80K) using the 70-Ti fixed angle rotor (Beckman Coulter), which can be described as follows. First, cell culture samples were centrifuged for 10 min at 300g and 4˚C to isolate cells, the supernatant was collected and spun for 10 min at 2,000g and 4˚C to isolate dead cells, the supernatant was centrifuged for 10 min at 10,000g and 4˚C for to isolate cell debris, then the supernatant was taken to

isolate EVs by ultracentrifugation for 70 min at 100,000g and 4˚C. The supernatant was removed, and the pellet was resuspended in PBS for a final washing step that lasted 70 min at 100,000g and 4˚C in order to remove protein contaminants in the supernatant. The final EV pellet was resuspended in the volume needed for subsequent experiments.

Initial EV detection by ELISA:

Tissue culture supernatants were analyzed for their CD63 expression following ultracentrifugation using a rat CD63 sandwich ELISA kit (LSBio LS-F20381). Briefly 100 µL reconstituted EVs from 24-, 48-, 72-, and 96-hours culture timepoints were placed in the ELISA well and incubated for 2 hours at 37^{O}C, the solution was aspirated, and a biotinylated antibody detection reagent was added and incubated for 1 hour at 37^{O}C. Wells were washed three times with the included kit wash buffer before adding a streptavidin-HRP complex detection reagent to bind to the antibody and incubated for 1 hour at 37^{O}C. Wells were washed five times with buffer before adding 90µL TMB substrate and incubated for 10-20 minutes at 37^{O}C before adding 50 µL of kit stop solution. The plate was analyzed for its optical density values using a spectrophotometer (BioTek SN2006877) plate reader set to 450 nm. A standard curve was formed from the provided kit standards and used to estimate values from EV samples.

Detection and Estimation of EVs by Flow Cytometry:

Fresh tissue culture supernatants were collected 96 hours after media was changed and EVs were harvested via ultracentrifugation. The EV pellet was resuspended in multiples of 50 µL PBS as needed for splitting samples for acquisition, with 50 µL being a 1X dilution. Following dilution, samples were transferred to a new 5mL poly propylene

round-bottom tube (Falcon 352063). 50 µL PBS staining solution was added to each tube containing either fluorophore: 0.6 µg CD63 APC (Miltenyi Biotec 130-108-833), 0.6 µg CD9 PE (Biolegend 206507), or a non-stained PBS sample for a final 100 µL staining volume. Prior titration experiments were used to determine the ideal EV and antibody dilutions for characterization to decrease swarm effects (particles coincidences) and achieve single particle detection. The final 100 µL staining volume was incubated in the dark at room temperature overnight, then the tube volume was increased to 400 µL with PBS the following morning. Appropriate EV dilutions were made serially based on previous titration experiments. After EVs were diluted, acquisition was run on the spectral flow cytometer (Cytek Aurora) utilizing violet laser side scatter height to detect particles as small as 90 nm. After acquisition, volumes and event rates were determined and the number of particles per flask were back calculated (n=4) and normalized to the SVF cell count taken after media collection. This methodology allowed for an estimation of the number of particles secreted per SVF cell in 96 hours.

Flow Cytometer Instrument set-up and Analysis:

Extracellular vesicles (EVs) were analyzed on a spectral flow cytometer Cytek Aura capable detecting particles as low as 90nm, equipped with 3 lasers (violet (405 nm), blue (488 nm) and red (640 nm)) and 38 detection channels. Instrument threshold was set using side scatter of the violet laser that had a superior focusing, as compared with the blue laser side scatter. The violet side scatter threshold was set to 800. The threshold value was established aiming less than 40 events per second on a low flow rate in the buffer control. To allow required sensitivity for the small particle detection, voltages on all 3 lasers were increased by 200% from the default Cytek settings. EVs titrations were

performed to decrease swarm effects (particles coincidences) and to achieve single particle detection. Data for each sample were acquired for 2 minutes per sample with a low flow rate. Obtained data were analyzed utilizing SpectroFlo and FlowJo software. Media controls were utilized to set gates for the data analyses.

Preparation of Gelatin Methacrylate dual crosslinked hydrogels:

Gelatin methacrylate (GelMA) was crosslinked along two axes as previously described [35, 37]. Briefly, six and eight percent (w/v) gelatin methacrylate hydrogels were synthesized by dissolving the appropriate weight of gelatin methacrylate (Advanced Biomatrix #5208) in 1X PBS (Fischer 10-010-031) with 0.2% (w/v) irgacure photo crosslinking reagent (Advanced Biomatrix #5200) in the dark and incubated in a 37˚C water bath for ~5 minutes to liquify. Once the gelatin was dissolved, the solution was used to resuspend the cell/EV pellet in 200 µL gel volumes as need. SVF cells were added to gels at a concentration of 10^6 cells/mL, about 200,000 cells per gel [38], and approximately 1.84 x 10^8 EVs were added to 200 µL gels based on estimations made from flow cytometry results using 200,000 SVF cells in culture for 96 hours. After reconstitution of biologics, gels were then pipetted into a 96 well plate (Falcon, REF351172) and exposed to UV light at an intensity of $\geq$ 20 mW/cm^2 (UV light meter model 06-662-65, S/N 51199975) for 1 min to crosslink methacrylate side groups (Blak-Ray longwave ultraviolet lamp UVP model B 100A, 115 V, 60Hz, 2.5 Amps 95-0044-22M), gels were then transferred to a pre-weighed 48 well plate (Corning, REF3548) and then weighed again—see degradation testing. After transfer, each hydrogel was supplemented with microbial transglutaminase (mTG) to crosslink lysine and glutamine side groups (sigma SAE0159) at a concentration of 10 U/g of gelatin for two hours in

PBS at 37ºC. The solution was removed, and the gels were washed three times with PBS for five minutes. After washing, biologic free gels were incubated in 1X PBS at 37˚C in 5% CO_2 throughout degradation testing and biological gels were incubated in DMEM (10% FBS, 1% Pen/Strep) at the same conditions. See Figure 1 below.

Hydrogel degradation and analysis:

Hydrogel degradation was determined solely based on the properties of the dual crosslinked gelatin methacrylate hydrogels without biologics *in-vitro*. To determine degradation, 48 well plates used for culture were pre-weighed prior to gel synthesis and weighed again after gelation. PBS was changed every six days and the plate was reweighed after removal of the PBS solution. Percent weight change was plotted over time to generate a degradation curve. A single two parameter exponential decay regression was fitted to the data using SigmaPlot 14.0 (Systat, San Jose, CA, USA) to determine if either gel decayed at a significantly different rate using the following differential equation one below, which when solved becomes equation two that was fitted to the data:

$$\frac{dW}{dt} = -k_d W \tag{1}$$

$$W = W_0 e^{-k_d t} \tag{2}$$

Where W is the percent weight change, k_d is the degradation rate, t is time in days, and W_0 is the initial percent weight.

Verification of biological gels:

Addition of biologics to gels was verified via confocal microscopy using a Nikon C2+ inverted microscope (Melville, NY, USA). SVF laden hydrogels utilized cells harvested from GFP+ rats, therefore cell laden and blank hydrogels were imaged at 488 nm to verify successful encapsulation of cells into the gel. Blank gels were imaged as a control. Gels were placed on a micro cover glass slide (24x60 mm no. 1.5 VWR 48393-251) above the objective on the inverted scope to allow for rotation of gels and capture images from multiple sides.

EVs were stained with PKH26 red membrane dye (Sigma MINI26) prior to gel fabrication according to manufacturer instructions, by diluting the dye 1:250 in the provided diluent and incubating with the EV sample for 5 minutes and then quenched using serum media solution (DMEM/FBS). The EVs were pelleted via a 100,000g spin for 60 minutes at 4˚C, washed with 1X PBS, recentrifuged at the same conditions, and resuspended in the volume of GelMA needed for gels. After enzyme incubation, gels were imaged using the 555 nm laser. Stained media that was not in contact with cells underwent the same ultracentrifugation and staining procedures before being encapsulated into gels to be used as an imaging control.

Viability of Biological gels:

To verify that the synthesis of GelMA hydrogels was not cytotoxic, a blue/red viability kit (Invitrogen R37610) was used to stain the SVF cells following isolation, SVF cell-laden hydrogels immediately after fabrication, and 24 hours post fabrication. Briefly, gels were incubated for 15 minutes in 1mL of media containing 2 drops of the NucBlue reagent, imaged using the DAPI filter, and 2 drops of Propidium Iodide reagent, imaged using the TRITC filter. Cells were incubated similarly but were mounted on with

fluroromount and cover slipped with micro cover glass slide (24x60 mm no. 1.5 VWR 48393-251). Immediately after staining, the gels were washed three times with 1X PBS for five minutes and placed on a micro cover glass slide (24x60 mm no. 1.5 VWR 48393-251) above the objective to image on the Nikon C2+ inverted microscope (Melville, NY, USA) using the 20X objective, relative to a blank stained control gel. 12 representative images were taken of the initial cell population, due to lower cellular presence in the field, and six representative images were taken on different sides of each subsequent gel. Percent viability of the gels calculated and graphed.

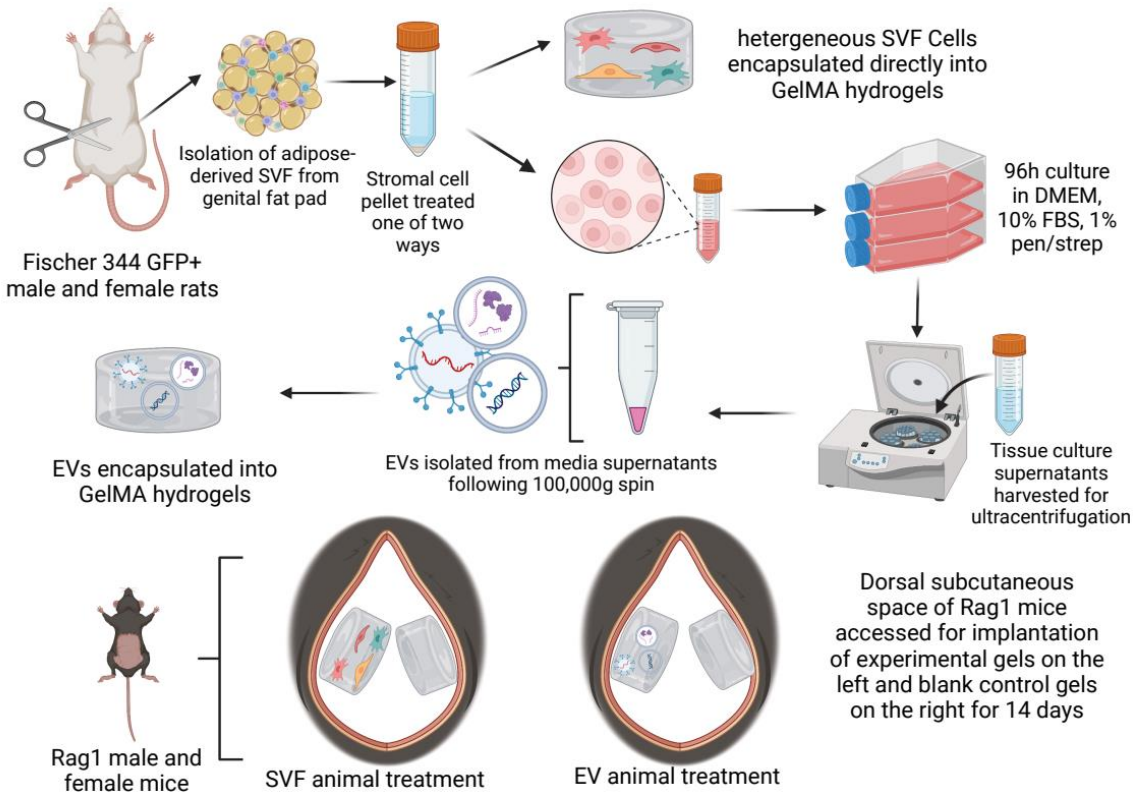

Figure 1: **Schematic of methods.** schematic showing methods for harvesting GFP+ SVF from Fisher 344 male and female rats before encapsulation into gels. Also represented is the culture of cells to produce EVs and their encapsulation in GelMA following ultracentrifugation. Methods were devised to ultimately implant experimental gels into a Rag1 mice model, shown at the bottom. Figure made with Biorender.com

Release of Biologics:

To provide some insight as to how the non-cellular gels may provide a therapeutic benefit, EVs were stained with PKH26 prior to gel synthesis as described above (n=4). After enzyme incubation, gels were transferred to a 48 well plate where they were supplemented with 1mL PBS. PBS was collected on day 7, centrifuged at 12,000g for 5 min to pellet gelatin clumps and the supernatant was analyzed using spectral flow cytometry (Cytek Auroa). Detection/quantification was aimed to assess if EVs are staying encapsulated in gelatin methacrylate or leeching out into the environment relative to non-stained EVs, as well as stained and non-stained media control samples which underwent ultracentrifugation and gel synthesis. This observed release was further confirmed by microscopy images taken on the Nikon C2+ inverted microscope (Melville, NY, USA) on day 7 to determine if EVs were still present in gels using the 60X objective.

in-vitro assessment of hydrogels:

A plug-in-field protocol was used to assess the revascularization potential of the gels *in-vitro* across tissue interfaces as previously described [39]. The plug was the 6% (w/v) dual cross-linked gelatin methacrylate hydrogels containing either cells, EVs, or blank control gels as described above. The field was 6% (w/v) gelatin methacrylate gel periphery cross-linked only by UV photolithography containing SVF cells at a density of 1 million cells/mL. Briefly, the plug was synthesized as mentioned above in a 96 well plate containing the appropriate biologics. EVs going into plugs were stained with PKH26 prior to synthesis to visualize EVs present in the plug and field, therefore a non-GFP+ rat source was used for the SVF cell field in these constructs, including their controls, to free up channels for staining. Groups can be summarized as follows:

1. GFP+ SVF cell plugs with GFP+ SVF cell fields + blank control plugs with GFP+ SVF cell fields- stained for DAPI, GFP, GS1-Rhodamine, and αSMA (day 7 and day 14).
2. PKH26 labeled EV plugs with non-GFP+ SVF cell fields + blank control plugs with non-GFP+ SVF cell fields- stained for DAPI, GS1-Fluroecein, prelabeled PKH26, and αSMA (day 7 and day 14).

After plug synthesis, the gels were then taken out of the wells and transferred to a 48-well plate, where 400 µLs of 6% GelMA/Cell solution was added to the periphery and cross-linked with UV lights for 1 min, as described above. See Figure 2 below. Once gelled, each well was supplemented with 0.5 mL DMEM, 10% FBS, and 1% Penicillin Streptomycin, which was changed every other day. On day 7 and 14 the plug-in-field gels were removed from the 48 well plate and frozen immediately in OCT. 100µm cryo-sections were taken from the OCT embedded constructs onto VWR micro slides (48311-703), air dried overnight, stored in -20^{O}C until needed, and stained as described below in the staining of SVF and SVF-EV *in-vitro* constructs.

Antibody pilot study for staining:

Pilot staining was done using the protocol detailed in the section below. Samples were pulled from day 14 SVF and EV experimental groups using 2 separate slides per stain tested, one slide receiving the stain and one slide not stained. All slides received DAPI. SVF slides were tested for GFP+ expression with rabbit anti-GFP (Millipore AB3080) diluted 1:100 with Alexa Fluor 488 goat anti-rabbit (Invitrogen A11034) secondary antibody diluted 1:200, Griffonia Simplicifolia Lectin I (GS1)-rhodamine (Vector RL1102), and mouse anti- α- smooth muscle actin (α-SMA) (Millipore A5228)

diluted 1:100 with Alexa Fluor 647 goat anti-mouse (Jackson ImmunoResearch 115605003) secondary diluted 1:200. EV constructs were tested for GS1-Fluorecein (Vector FL1101) (488), and mouse anti- α- smooth muscle actin (α-SMA) (Millipore A5228) diluted 1:100 with Alexa Fluor 647 goat anti-mouse (Jackson ImmunoResearch 115605003) secondary diluted 1:200. Controls did not receive primary antibody but were treated with the secondary antibody. Controls did not receive the GS1 stain. All images were taken on Nikon C2+ inverted microscope (Melville, NY, USA) using the 10X objective full field for GS1 stains and the 10X objective + Nyquist resolution for GFP and αSMA stains. Initial antibody pilot studies required antigen retrieval of GFP and αSMA stains, but not of GS1 stains.

Staining of SVF and SVF-EV *in-vitro* constructs:

Frozen sections were removed from -20^{O}C storage and air dried at room temperature for 1 hour prior to staining. The slides were washed two times for five minutes with 1X PBS to remove excess OCT, then fixed for 15 min in 4% Paraformaldehyde solution (Electron Microscopy Sciences 157145), followed by a five-minute wash in PBS. Following fixation, slides underwent antigen retrieval steps using a 1X Antigen retrieval acidic reagent (R&D systems CTS014) according to manufacturer's instructions. Samples were incubated in the reagent for five minutes at 92ºC and were then washed for five minutes with deionized water and then PBS. Sections underwent blocking-permeabilization steps in 4% goat serum (Invitrogen 31873), 0.5%Triton X-100 (Sigma T-8787) solution in PBS for 2 hours. All antibodies and lectins were diluted in 200 µL blocking solution. After removal of blocking solutions, SVF constructs were stained with rabbit anti-GFP (Millipore AB3080) diluted 1:100 and mouse anti-αSMA

(Millipore A5228) diluted 1:100 primary antibodies and incubated overnight at 4ºC. The next morning, slides were washed three times each with PBS for five minutes and incubated in 200 µL secondary solutions containing: Alexa Fluor 488 goat anti-rabbit (Invitrogen A11034) diluted 1:200, GS1-Rhodamine (Vector RL1102) lectin diluted 1:40, and Alexa Fluor 647 goat anti-mouse (Jackson Immunoresearch 115605003) diluted 1:200 for an hour and fifteen minutes at room temperature for SVF constructs. After secondary/lectin incubation, the slides were washed with PBS for 10 min, incubated 20min with PBS and two drops of DAPI staining solution (Invitrogen R37606) and washed 10 minutes afterward with PBS. Sections were mounted in fluoromount (#0100-01), cover slipped with micro cover glass slide (24x60 mm no. 1.5 VWR 48393-251) and allowed to be fixed overnight prior to imaging. Similarly, after removal of blocking solutions, EV constructs were stained mouse anti-αSMA (Millipore A5228) diluted 1:100 primary antibodies, along with prelabeled PKH26 EVs. As for secondary antibodies, EV constructs were stained with GS1-Fluorecein (Vector FL1101) diluted 1:40 and Alexa Fluor 647 goat anti-mouse diluted 1:200. A non-GFP+ source rat animal was used for SVF cell fields of EV plug-in-field experiments. Control plug-in-field gels were stained the same as their respective experimental gels. All images were taken on the Nikon C2+ inverted microscope (Melville, NY, USA) using the 10X objective + Nyquist resolution.

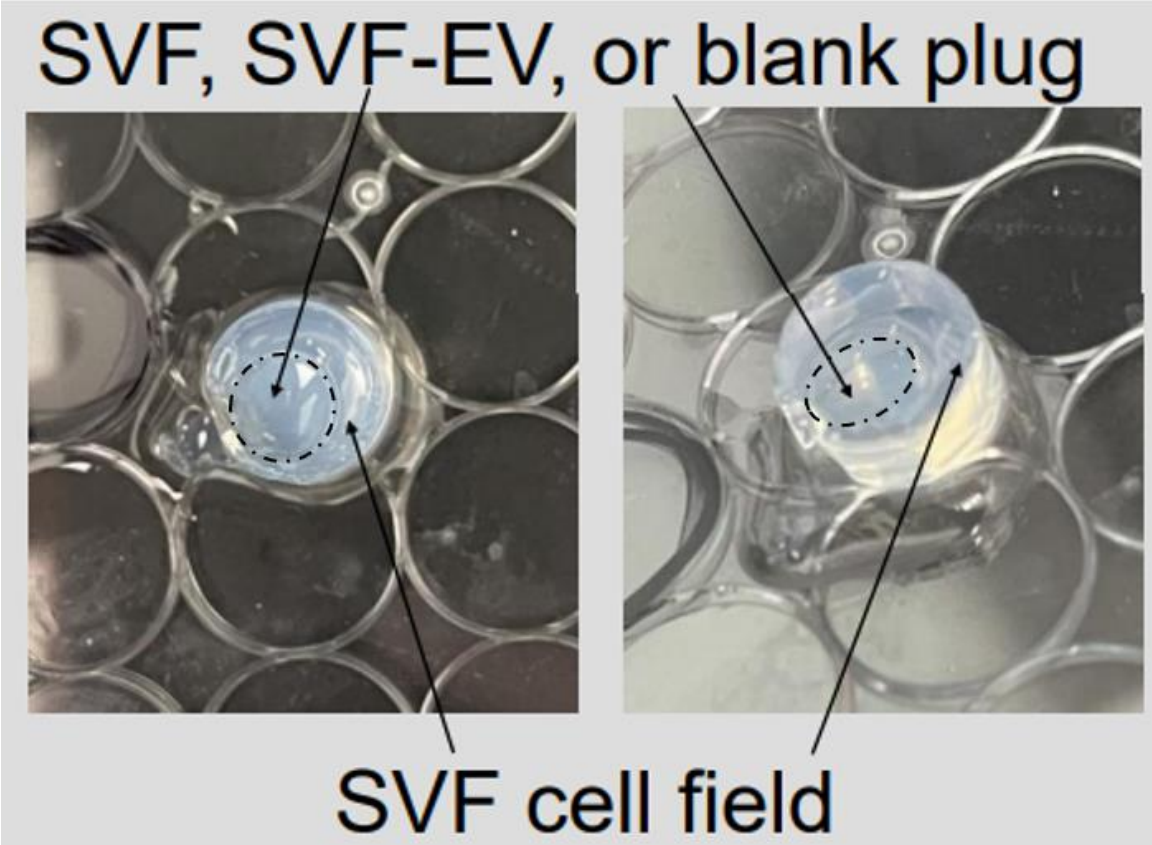

Figure 2: **Plug-in-field gels.** Plug-in-field gels used to assess vasculogenic potential of hydrogels containing either a SVF, SVF-derived EV, or blank hydrogel plug, surrounded by a SVF cell field, which were made by first synthesizing the dual crosslinked GelMA plug, then crosslinking the outer cell field using only UV light. Constructs were harvested and imaged at 7- and 14-day timepoints.

In-vivo Implantation of hydrogels:

2-month-old male and female Rag1 mice (Jackson Laboratory) were weighed, anesthetized via 3% isoflurane, and the dorsal area around the hindquarters was shaved. Animal surgical areas were prepped with ethanol, betadine, and saline, following aseptic surgical technique. An incision was made laterally along the midline ~1-2 cm from the posterior end of the mouse that was wide enough to fit the construct. The area above the facia layers was blunt dissected to access the subcutaneous space on either the eft or right side of the animal. Once the space was open, either a SVF cell (n=5) or EV (n=5) gel was placed on the left side of the animal and a blank control gel (n=10) was placed on the right side of the animal. The incision was closed with 4-0 polypropylene sutures (Ethicon 8682) and staples were used overtop of the sutures. Animals were administered 20 mg/kg meloxicam (VetOne Ostilox VT501080) on surgery day and each day for 48 hours after surgery. After 14 days, the animals were anesthetized under 3% isoflurane and administered 200 µL dextran tetramethyl rhodamine (Invitrogen D7139) at a concentration of 5mg/mL in saline via a jugular cutdown (about 1.5 inches longitudinally on the neck). The jugular vein was isolated from surrounding muscle and fascia where the solution was injected using a 30G needle (BD PrecisionGlide 305106) and allowed to circulate for 15 minutes. During this period, animals underwent Laser Doppler Imaging (LDI) (MoorLDI model MOORLDI2-IR-HR) of the dorsal hindquarters where gels were present to visualize surface blood flow. After 15 minutes the animal was euthanized by cervical dislocation while still under isoflurane, and the gel constructs were explanted by cutting the connective tissue layers around the gel. Explants were washed in 1XPBS for 5 minutes, and frozen in OCT. The embedded constructs were cryo-sectioned at 100 µm

thickness onto VWR micro slides (48311-703) and imaged to quantify vascular density between the cell, EV, and control groups. SVF groups were stained for DAPI, GFP, and α-smooth muscle actin (αSMA); EV groups were stained for DAPI, GS1-Fluorecein, and αSMA, according to the same staining protocol detailed above. All Groups were assessed for Dextran expression using the 555 nm laser. All images were taken on the Nikon C2+ inverted microscope (Melville, NY, USA) using the 10X objective + the same Nyquist resolution as plug-in-field studies for the same final magnification *in-vitro* and *in-vivo*.

Image Analysis:

In-vitro images were analyzed by quantifying cell populations in the plug and for all groups and were further assessed for which of these cells were expressing GS1 markers of endothelial cells or αSMA. Three representative 10X images were taken for each replicate and averaged to give a final value for each n, which was then analyzed across groups using a one-way analysis of the variance (ANOVA) on ranks by the Kruskal-Wallis and Dunn's methods ($\alpha=0.05$).

In-vivo images were analyzed by overlaying DAPI and Dextran filters to visualize perfused blood vessels present in the gels following explant. These images were further analyzed in ImageJ Fiji software where the pixels were scaled to the appropriate unit in microns, converted to 8-bit, adjusted to an appropriate threshold value to fill in the vessels appropriately on the grayscale image. A shape filter plugin was used to remove single nuclei from the image, and the image was converted to binary where the percent vascular area was calculated by the software, as previously described [28, 39]. Three representative 10X images were taken for each replicate and averaged to give a final value for each n, which was then analyzed across groups using a one-way analysis of the

variance (ANOVA) on ranks by the Kruskal-Wallis and Dunn's methods (α=0.05). Groups were also broken down into sex categories to compare the percent vascular variance between male and female groups. A one-way ANOVA pairwise comparison using the Holm-Sidak method was employed to assess the male groups *in-vivo* rather than the Kruskal-Wallis and Dunn's method due to the data set being normally distributed.

Image acquisition:

All images were taken using the Nikon C2+ inverted confocal microscope using various objectives as described for different experiments. Laser intensities and gain values were determined for each stain on the appropriate objective and maintained throughout imaging and across experiments. For example, 10X images of plug-in-field *in-vitro* constructs were imaged at the same laser settings for DAPI, GFP, GS1, and αSMA with the same Nyquist resolution as *in-vivo* hydrogels. Furthermore, settings were established by using the saturation indicator on the Nikon Elements software to ensure minimal pixel saturation was present in samples in order to reveal true signal. Control stains as well as control groups were employed as well to ensure true signal was being represented accurately in all images at the appropriate settings.

Statistical Analysis:

Statistical Analyses were performed in SigmaPlot 14.0 (Systat, San Jose, CA, USA) with $p < 0.05$ as the significance level.

RESULTS

Hydrogel Degradation:

Degradation experiments were conducted at physiological pH to assess which concentration of GelMA would provide a prolonged degradation of the biomaterial among six and eight percent hydrogels. The percent weight change of the biomaterial over time is presented in Figure 3 below. The final percent weight retained on average after 60 days for six percent gels was ~78% and was ~79% for eight percent gels, suggesting prolonged degradation. Exponential regressions revealed strong similarity to the degradation rate of the two concentrations of gelatin methacrylate (0.003/day for 6% gels and 0.0031/day for 8% gels). See Figure 4. Furthermore, the degradation profiles appear to be somewhat sharp the first 10 to 20 days in physiological solution, but then plateaus for the remaining experimental timeframe. Other literature sources have previously determined that increasing percentages of gelatin methacrylate result in lower cell viability [40], therefore, six percent gels were chosen for the remaining experiments.

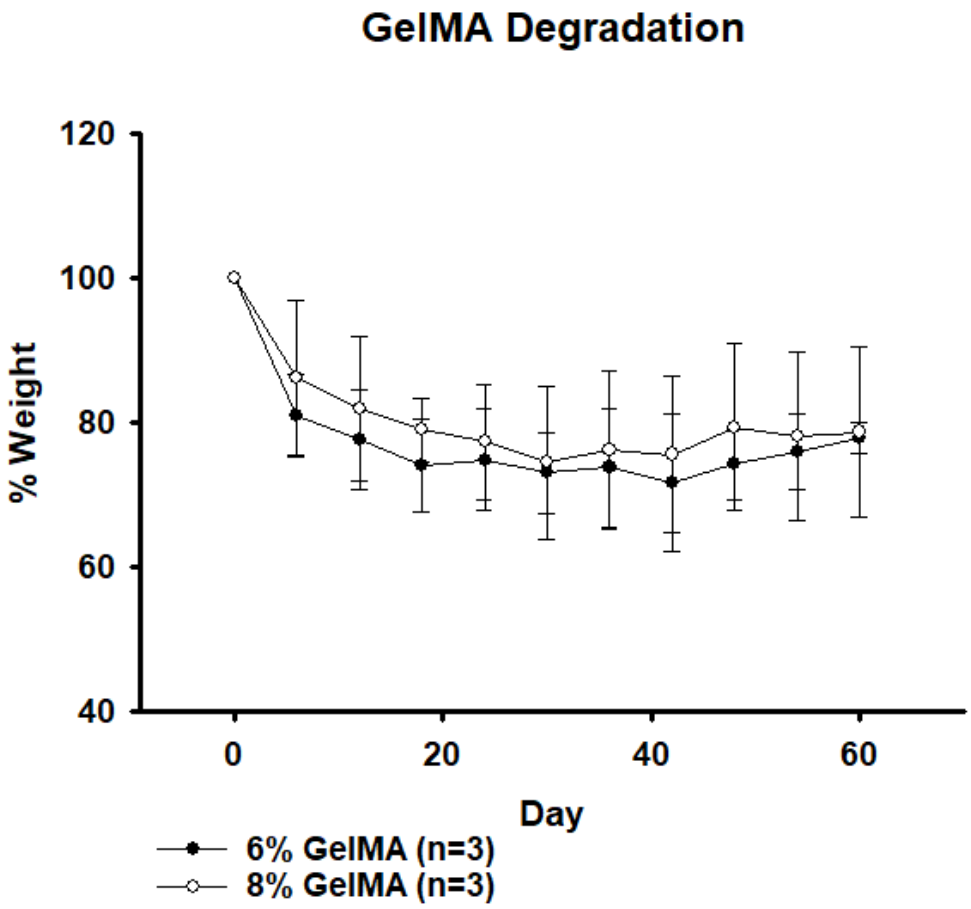

Figure 3: **GelMA degradation.** Graph of percent weight change of six or eight percent gelatin methacrylate hydrogels in PBS over 60 days (n=3), data was graphed following the completion of degradation experiments. Results verified a prolonged degradation of the gels *in-vitro* by retaining near 78% percent of the gel weight on average on day 60 for six percent gels and 79% for eight percent gels, with error bars showing the positive and negative standard deviation of the data set per day.

6% Regression

R	Rsqr	Adj Rsqr	Standard Error of Estimate
0.4806	0.2310	0.2062	8.1741

	Coefficient	Std. Error	t	P
a	84.8996	2.7649	30.7065	<0.0001
b	0.0030	0.0010	3.1414	0.0037

8% Regression

R	Rsqr	Adj Rsqr	Standard Error of Estimate
0.4334	0.1878	0.1616	9.7990

	Coefficient	Std. Error	t	P
a	88.2277	3.3154	26.6112	<0.0001
b	0.0031	0.0011	2.7418	0.0101

Figure 4: **Regression analysis of GelMA degradation.** Regression analysis performed using SigmaPlot for a single two parameter exponential decay regression as described above, with b representing the k-value suggested in the regression model in the methods section. The R-squared values are poor for both groups, however similar numbers are reflected for the degradation constant of six and eight percent gels over the 60-day period, which suggest the gels are decaying at similar rates based on this model.

EV Detection by ELISA:

The CD63 ELISA was used to confirm isolation of EVs from cell culture supernatants following an established ultracentrifugation protocol. Results from ELISA suggested higher CD63 expression from 96 hours in cultures, relative to other timepoints. This expression alludes to higher EVs present in cell culture supernatants, so 96-hour time points were chosen for further experiments. However, none of the detected values from the spectrophotometer were within the standards provided by the kit, so this data could not be used to verify exosome isolation. To ensure a high presence of EVs in samples to be detected by flow cytometry, cell culture conditions were altered to those described in the methods using T-182 cm^2 flaks and a higher seeding density of ~25,000 cells/cm^2.

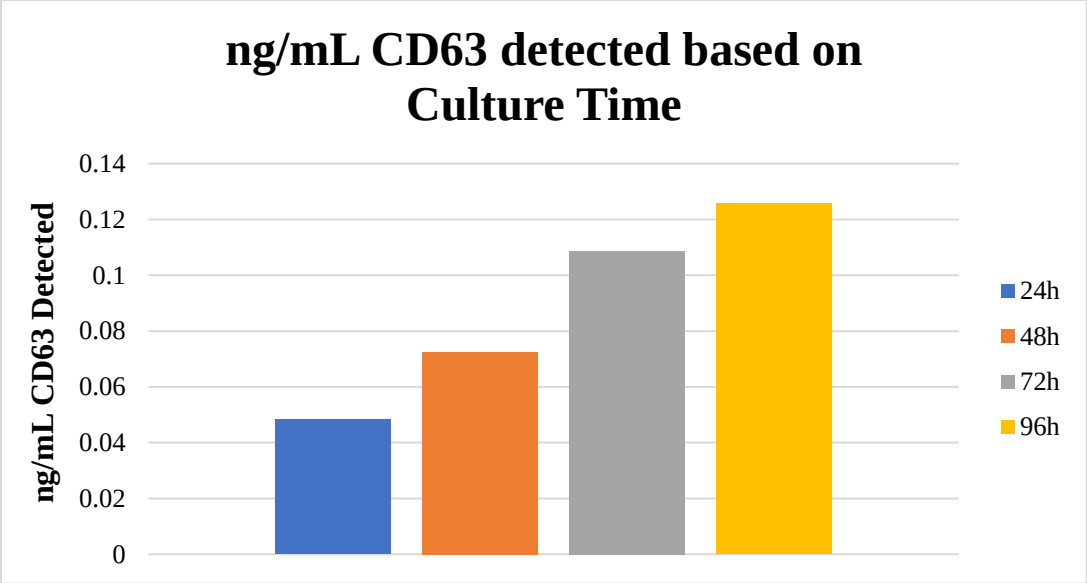

Figure 5: **CD63 ELISA results.** Results of ELISA used to detect ng of CD63/mL from cell culture supernatant following ultracentrifugation and EV reconstitution in 100 µL. Dilution factor one. Results suggested 96 hours culture time allowed for maximum EV secretion.

EV Detection by Flow Cytometry:

EV isolation by ultracentrifugation was confirmed via flow cytometry using cytokine markers CD63 and CD9 to identify components of cell culture supernatants formed by the endosomal pathway (n=4). Furthermore, flow cytometry was used to estimate the number of particles secreted from a known number of cells to correlate EV particle number with cell numbers cultured in a 96-hour time period. An EV titration experiment was performed to prevent particle coincidences and achieve single particle detection. Media controls were also analyzed in order to normalize particle counts to true EV signal. Additionally, antibody titration experiments were used to ensure optimal antibody concentration among samples and minimize aggregates from being detected. The final EV gating and detection for the markers, including controls, can be seen in Figure 6 below. Flow cytometry confirmed isolation of EVs from SVF tissue culture supernatants by ultracentrifugation and estimated ~920 particles secreted per cell in 96-hours which were characterized as being 53.5% CD63 positive and 20.5% CD9 positive (n=4), as indicated by table one below including the respective standard deviations. These results allowed for estimation of EVs which were loaded into GelMA hydrogels. EV hydrogels were synthesized from supernatants of 200,000 cells for 96 hours, which was estimated to be ~ 1.84×10^8 EVs in 200 µL gels.

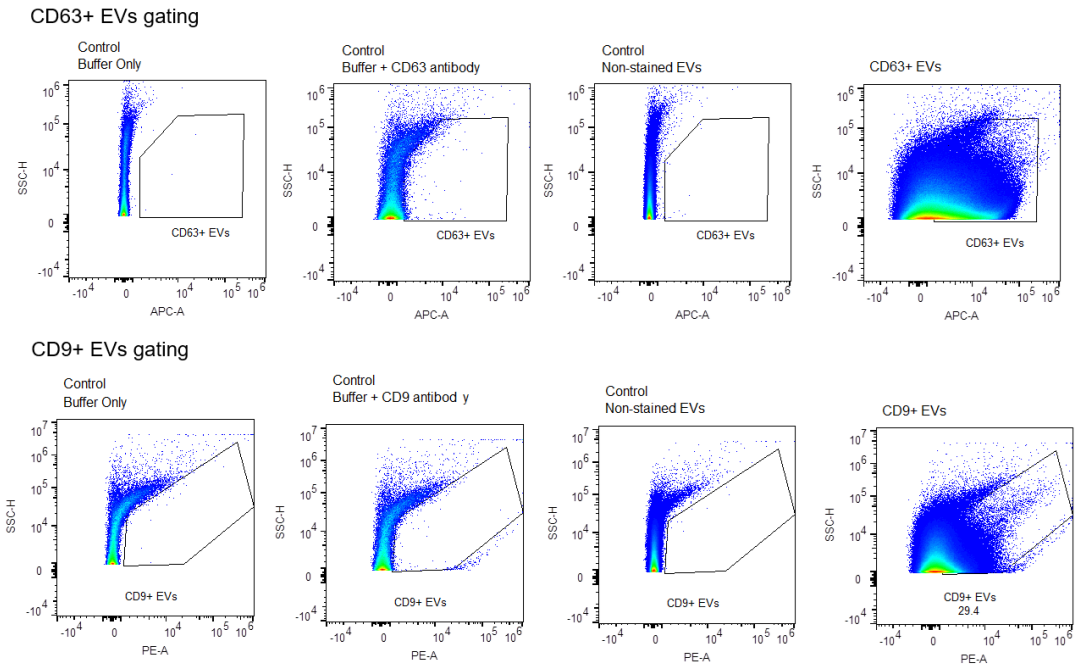

Figure 6: **EV detection by flow cytometry.** Dot plots demonstrate the gating CD63-APC and CD9-PE fluorophores used to identify EV populations relative to media buffer controls and non-stained EV samples using the SectroFlo and FlowJo software. Size and fluorescence confirm isolation of CD63 and CD9 positive EV populations.

Table 1: Final summary of EVs secreted per SVF cell number in 96h including cytokine expression (n=4).

Average EV per SVF cell in 96h (n=4) (+ StdDev)	± 95% CI	% CD63+ (+ StdDev)	%CD9+ (+ StdDev)
920.276 + 171.490	272.878	53.5 + 6.245	20.5 + 5.066

Verification of encapsulation:

Confocal microscopy images were used to verify the synthesis of biological gels using the Nikon C2+ inverted microscope. Following gel synthesis, GFP+ SVF cells could be visualized in a singular 20X imaging field relative to blank control gels (Figure 7), suggesting GelMA successfully encapsulates SVF cells. Furthermore, EVs were labeled with PKH26 membrane marker after ultracentrifugation and then encapsulated in GelMA for imaging. 60X images confirmed encapsulation of PKH26 EVs in a singular imaging field relative to a stained media control (Figure 9). To assess the three-dimensional distribution of biologics, the confocal microscope was used to image a small volume through the Z-plane. Images confirmed that the biomaterial can encapsulate both biological products needed for therapy in a 3-dimensional matrix, and images suggest even distribution of biologics throughout the hydrogel. See Figures 8 and 10 below.

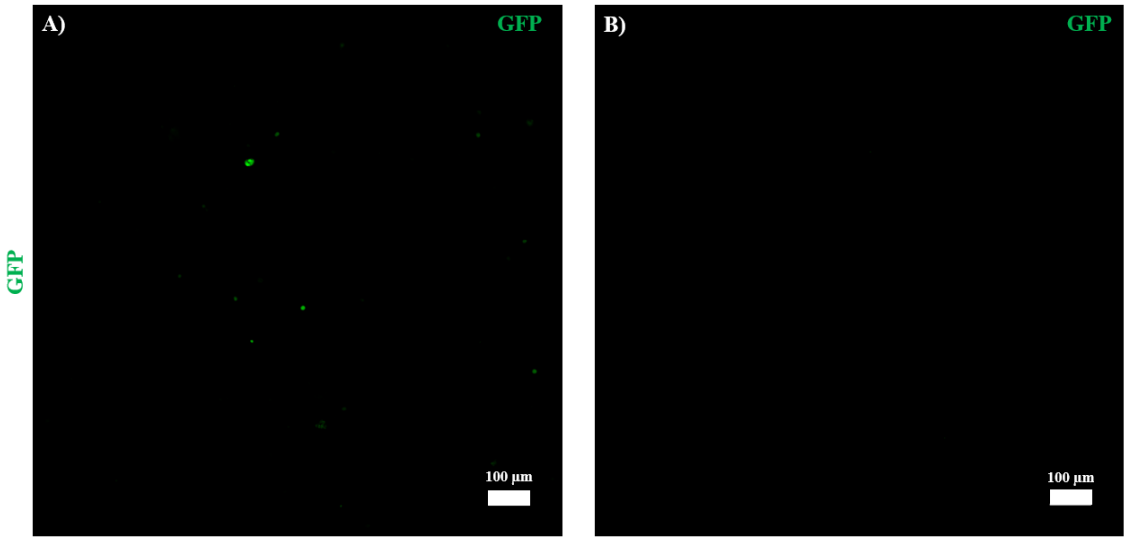

Figure 7: **GFP+ SVF cells encapsulated in GelMA.** 20X image field confirms encapsulation of A) GFP+ SVF cells in GelMA relative to a B) blank control field. Concentration is 1 million cells/mL in 200 µL gels. Scale bar 100 µm.

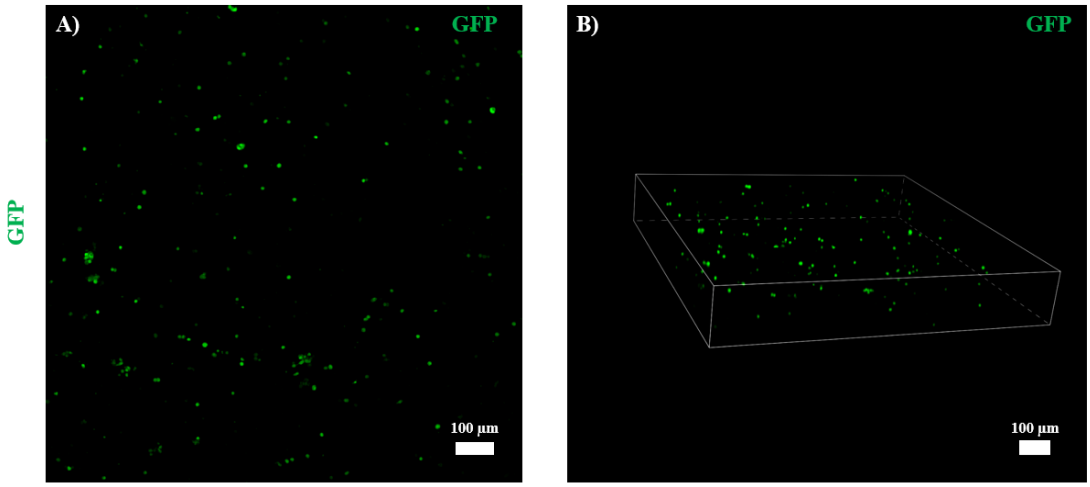

Figure 8: **GFP+ SVF cells encapsulated in GelMA volume.** 20X images display the A) maximum intensity projection compressed vertical stack image of 1 million SVF cells/mL encapsulated in GelMA through a small volume, B) displays the volume rendered confocal image of the z-stack pictured in "A)" and displays uniform distribution of cells throughout GelMA. Scale bar 100 µm.

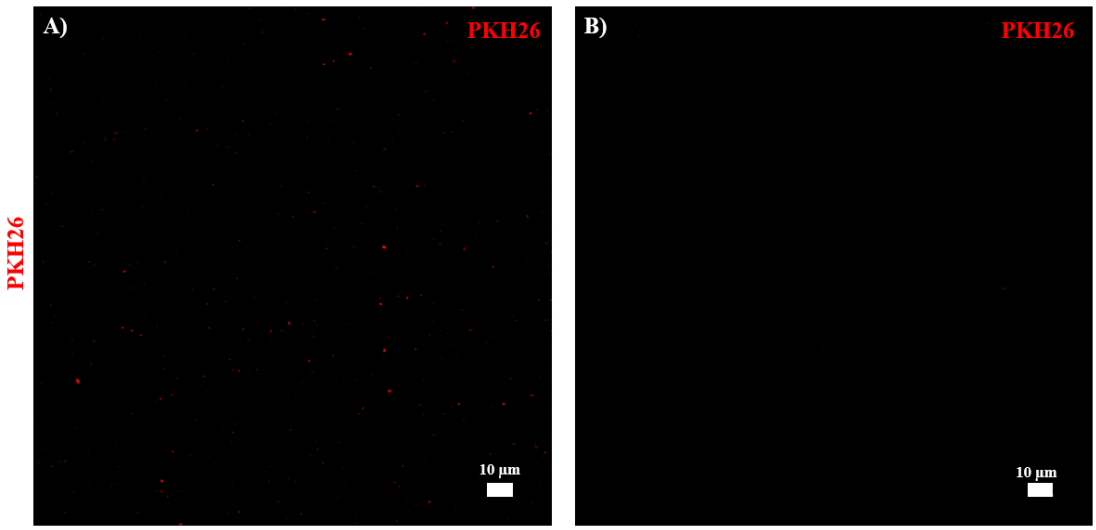

Figure 9: **PKH26 EVs encapsulated in GelMA.** PKH26 labeled A) EVs in a singular 60X imaging field compared to B) PKH26 labeled media. Scale bar 10 µm.

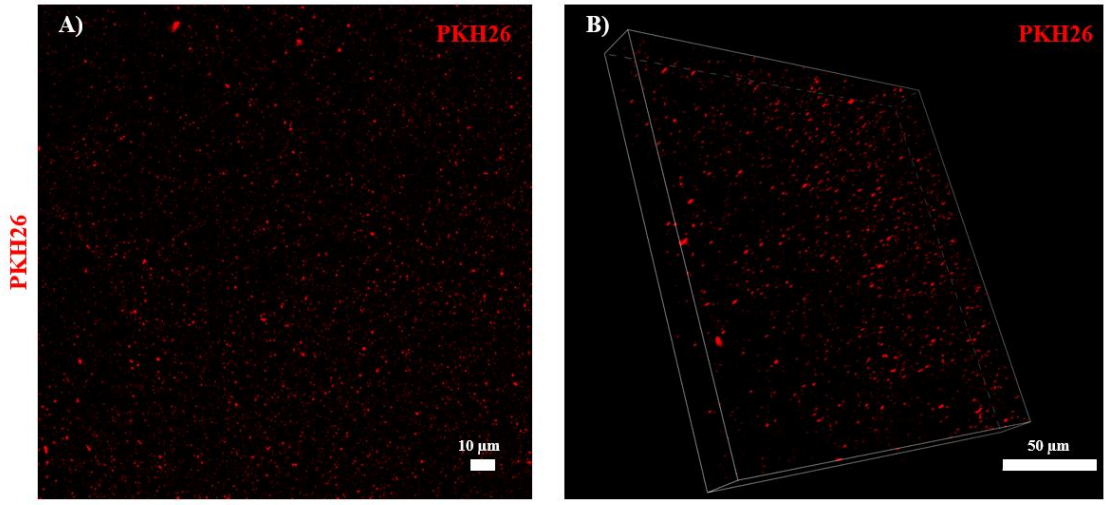

Figure 10: **PKH26 EVs encapsulated in GelMA volume.** 60X images displaying the A) maximum intensity projection of a compressed vertical stack image of PKH26 labeled EVs from 200,000 SVF cells in culture for 96 hours encapsulated in GelMA through a small volume (scale bar 10 µm), where B) displays the volume rendered confocal image of the z-stack pictured in "A)" showing uniform distribution of EVs throughout GelMA (scale bar 50 µm).

Viability of Biological gels:

GelMA hydrogels were further characterized by their level of biocompatibility. To ensure the gel synthesis process was not cytotoxic to cells, specifically the UV exposure, a blue/ red viability kit was used to quantify the percent viability of the initial cell population following a fresh isolation, then after gel synthesis, and 24 hours later. 12 representative images were used for the slide containing the stained cells resuspended in fluormount due to a lower cellular presence in the imaging field. Gels were placed on a micro-glass cover slide on the inverted scope and six representative images were taken per gel (two images on the bottom, two images on the top, and two images on the side). See Figure 11 below. Cell counts were performed based on the stain and revealed an above 98% viability on all cell populations before, after, and one day following fabrication, ensuring the gel synthesis process was not cytotoxic to cells. Specifically, the initial cell population showed 98.958% viability on average with 3.608% standard deviation, 98.401% viability on average after gel synthesis with 1.812% standard deviation, and 99.383% viability on average one day after fabrication with 1.512% standard deviation. See Figure 12.

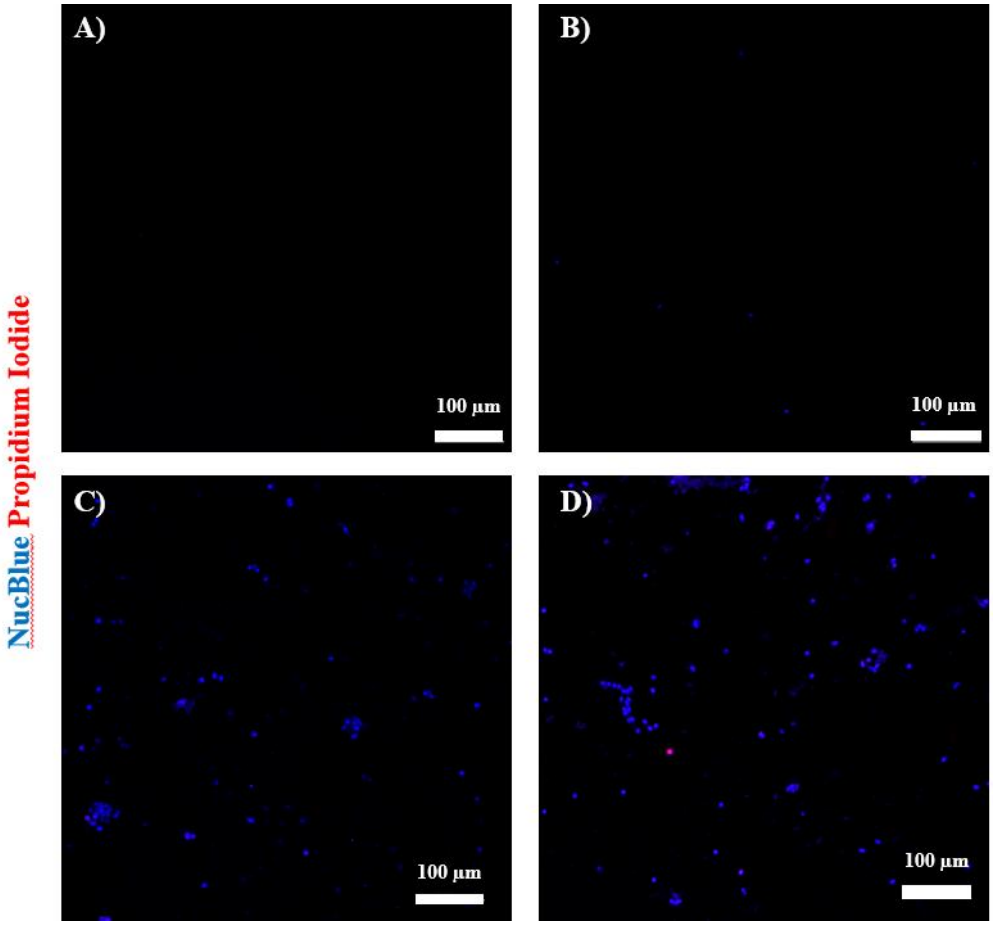

Figure 11: **Blue/red viability images of SVF in GelMA.** Stained SVF cells encapsulated in GelMA C) immediately following fabrication, and D) 24 hours post fabrication compared to A) a blank stained GelMA control, as well as B) the initial cell population isolated for gels. Where propidium iodide indicates dead cells and NucBlue live reagent labels cellular nuclei. Scale bar 100 µm.

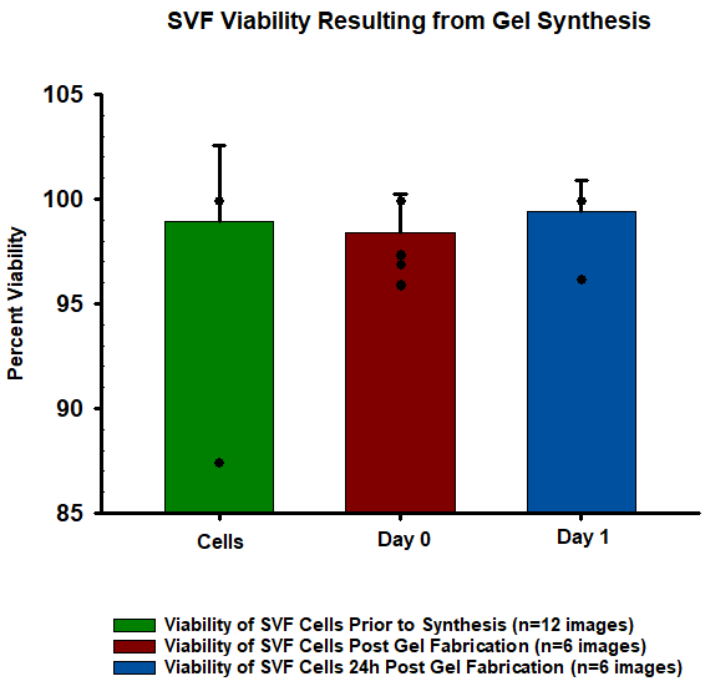

Figure 12: **SVF cell viability results of gel fabrication.** Average results from analysis of viability images comparing 12 images of the initial cell population mounted on a single slide against six images of stained GelMA constructs immediately after removal of mTG and 24 hours post fabrication. Results confirm viability of initial SVF isolation and continued viability after gel synthesis (>98% throughout). Specifically, the initial cell population showed 98.958% viability on average with 3.608% standard deviation, 98.401% viability on average after gel synthesis with 1.812% standard deviation, and 99.383% viability on average one day after fabrication with 1.512% standard deviation.

EV Release from biological gels:

Release studies were performed to determine how EV gels may provide a therapeutic benefit. PBS solutions incubating EV gels containing pre-labeled PKH26 EVs were harvested on day 7 and analyzed by flow cytometry to detect how many EVs were released over a week's time. Samples were analyzed relative to blank gels containing only media which underwent the same ultracentrifugation, staining, and synthesis process. Flow cytometry results revealed minimal, if any, release of EVs into the environment after a week's time (Figure 13). This observation was further confirmed by imaging the gels after one week and still visualizing a high concentration of EVs present in GelMA using the TRITC filter on the 60X objective (Figure 14). Results suggest therapeutic EVs are not releasing from gels and thus may be limited to the benefit they can provide to the surrounding tissue. Analysis from flow cytometry experiments were performed using SepctroFlo and FlowJo software.

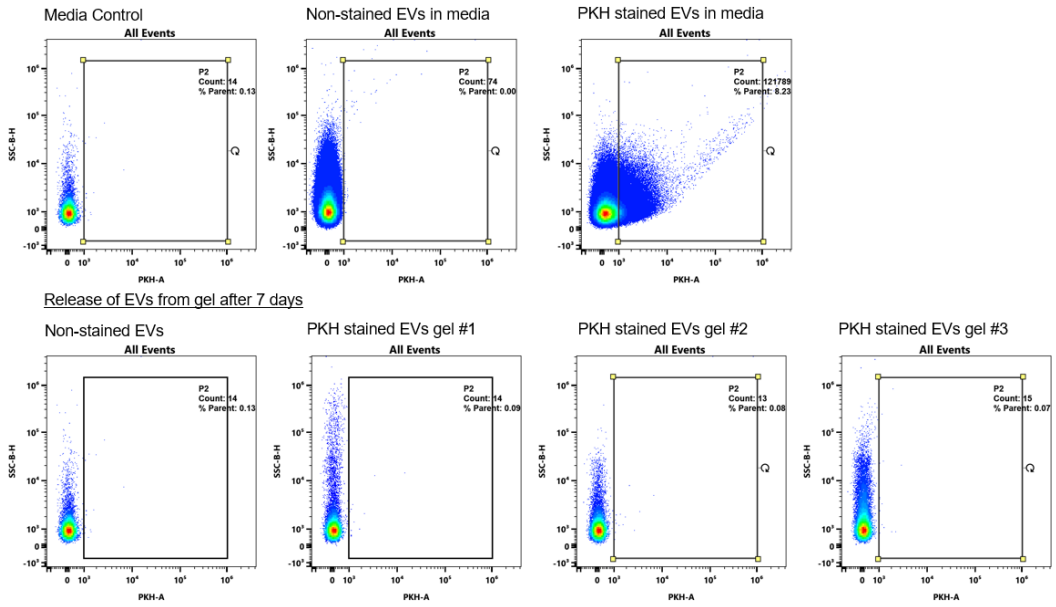

Figure 13: **Flow cytometry detection of released EVs.** Flow cytometry dot plots detecting PKH26 labeled EVs prior to being loaded into gels (top), and acquisition of PBS solutions containing released gel contents after seven days of incubation with prelabeled PKH26 EVs in GelMA (bottom). The absence of fluorescence in stained EV samples suggest EVs aren't releasing from gels after a week.

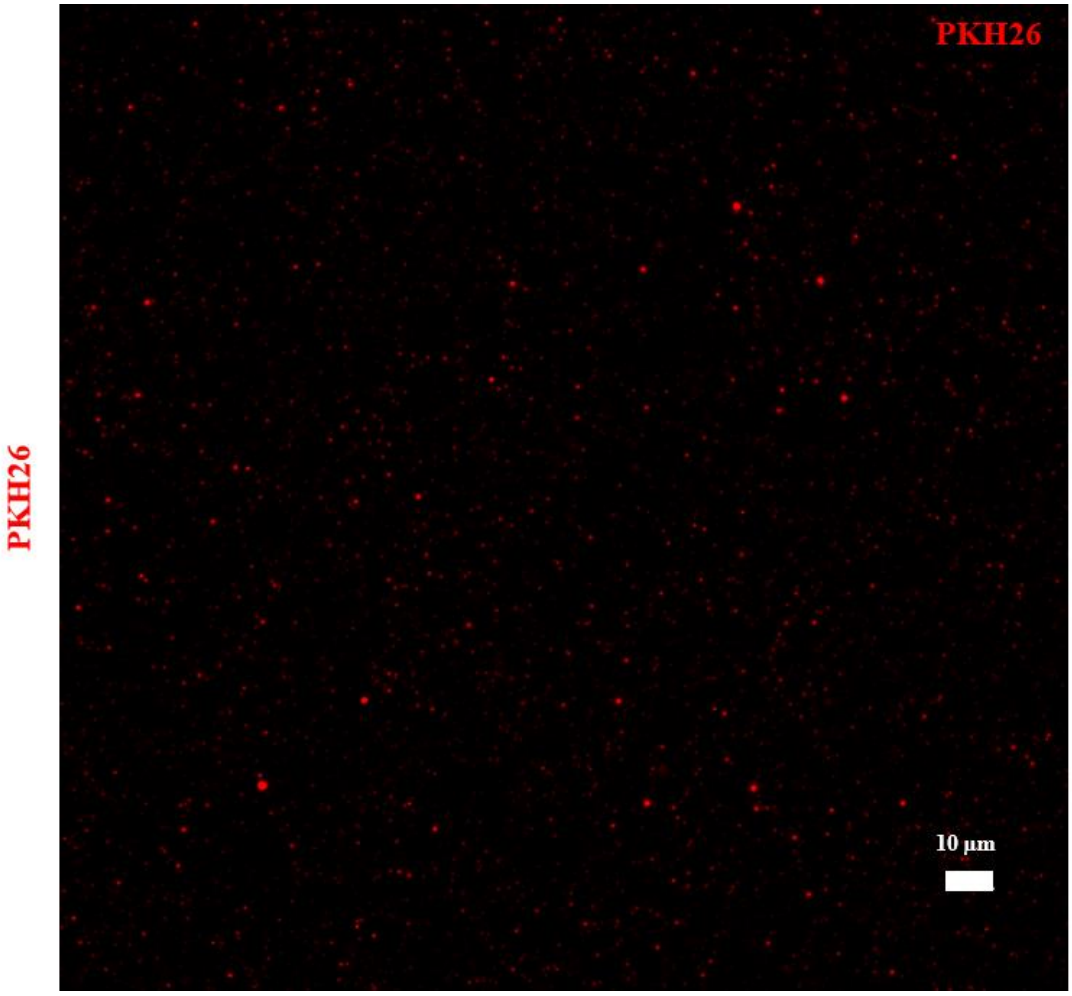

Figure 14: **Day 7 PKH26 EVs present in GelMA.** PKH26 labeled EVs in GelMA after seven days incubation in PBS. 60x compressed vertical confocal images through the Z-plane confirm flow cytometry findings that the EVs are still present in the gel after 7 days observationally similar to its loading concentration seen with initial verification images (Figure 10). Scale bar 10 µm.

Antibody pilot staining:

To ensure the staining hydrogels displayed true signal, the antibody pilot experiment used positive and negative controls of the appropriate markers, lectins, and dyes by adding the primary antibody, lectin, and dye to the positive control, and not using the reagent in the negative control. Results from microscopy images revealed strong signal among positive groups associated with cell expression using DAPI cell labeling. GFP and αSMA stains were imaged with the 10X objective + Nyquist resolution following antigen retrieval procedures, and GS1 images were taken using the full 10X field after confirming positive detection of the lectin without of antigen retrieval procedures. Based on the antibody pilot staining images expressing signal for positive controls and absence of signal in negative controls (Figures 15 and 16), the proposed staining procedure in the methods section above was used for GelMA hydrogels following *in-vitro* and *in-vivo* experiments.

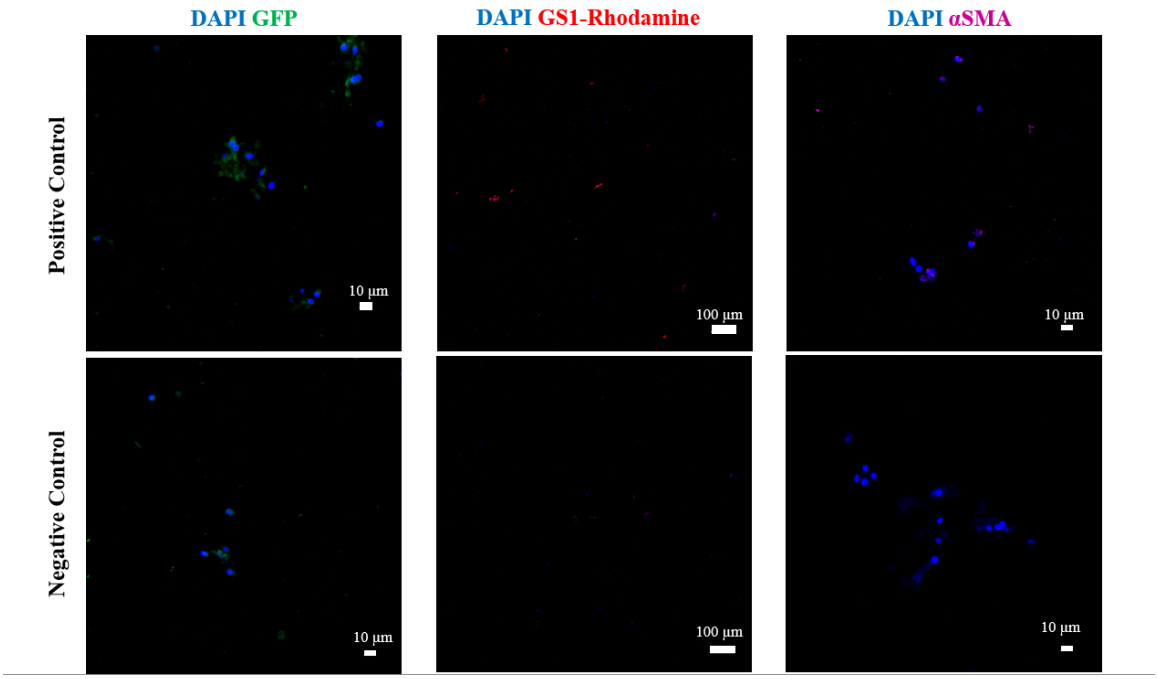

Figure 15: **Antibody pilot staining of SVF plug-in-field constructs.** Positive and negative control staining of day 14 plug-in-field SVF constructs to confirm accurate staining and imaging of GFP, GS1-Rhodamine, and smooth muscle actin expression. GFP and αSMA stains were imaged with the 10X objective + Nyquist resolution following antigen retrieval procedures (scale bar 10 µm), and GS1 images were taken using the full 10X field after confirming positive detection of the lectin without of antigen retrieval procedures (scale bar 100µm).

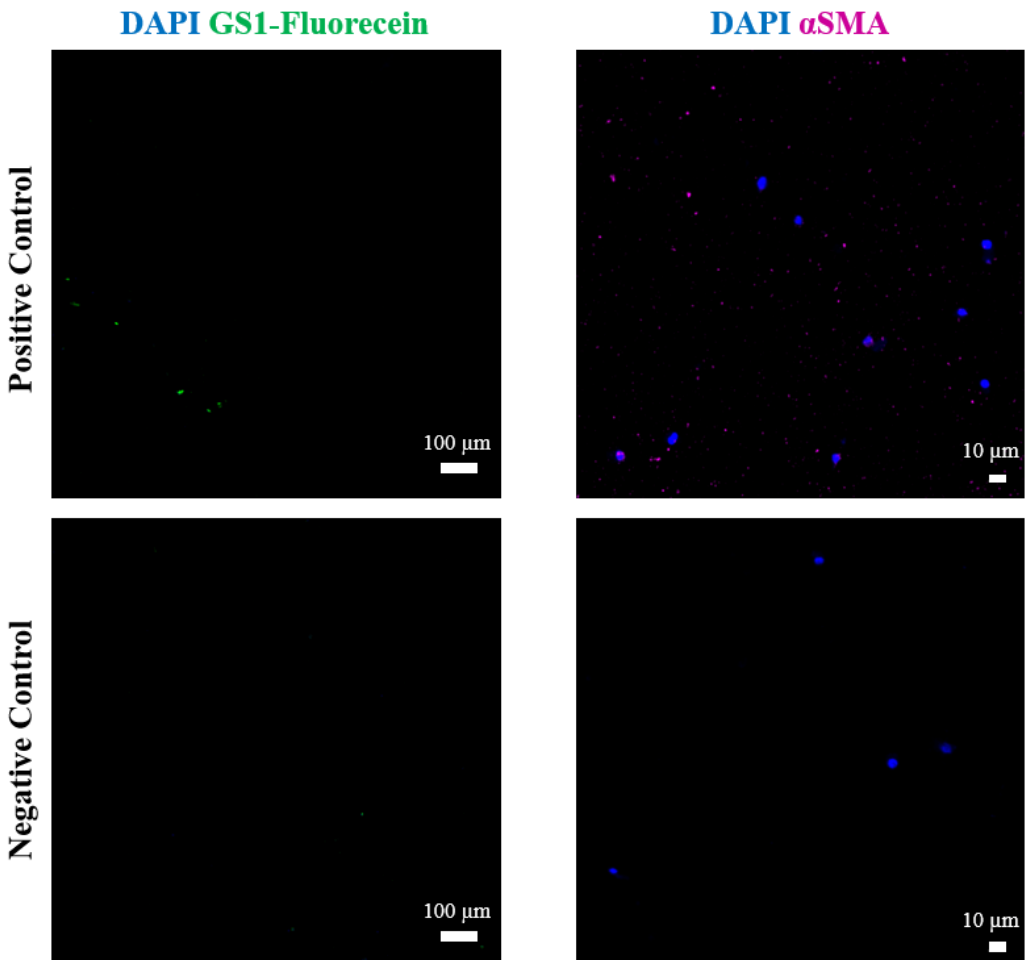

Figure 16: **Antibody pilot staining of EV plug-in-field constructs.** Positive and negative control staining of day 14 plug-in-field EV constructs used to confirm accurate staining of GS1-Fluorecein markers and smooth muscle actin. αSMA stains were imaged with the 10X objective + Nyquist resolution following antigen retrieval procedures (scale bar 10 µm), and GS1 images were taken using the full 10X field after confirming positive detection of the lectin without of antigen retrieval procedures (scale bar 100µm).

In-vitro plug-in-field:

The plug-in-field experiment was used to determine if the hydrogel constructs proposed here possesses the inherit ability to promote blood vessel formation spontaneously. SVF plug and fields did not display mature vascular tube formation after both 7- and 14-day timepoints (Figures 17 and 18). Some "tube-like" structures appear to be emerging in microscopy images, but mature tubes with connecting lumen between cells are not observed. Furthermore, EV plug and fields did not display vascular tube formation after both 7- and 14-day timepoints (Figures 19 and 20). However, the cell numbers present in therapeutic plugs differed across groups. A significantly higher cell population was observed in SVF plugs on day 7 compared to the control (Figure 21A) determined from the ANOVA analysis (α=0.05). The DAPI count of control plugs was an average of 0 with 0 standard deviation, EV plugs averaged 0.333 cells with a standard deviation of 0.272, and SVF plugs had an increased average cell count of 8.50 with a standard deviation of 3.272 on day 7. Percent expression GS1 and αSMA with DAPI labeled cells was also analyzed across SVF and EV groups (Figures 21B&C and Figures 22B&C), but neither group differed significantly from the other at either timepoint. However, the percent expression of GS1 increased from day 7 to day 14 with EV plugs going from an average 37.5% with a standard deviation 47.871% to an average 48.0% with a standard deviation 50.20%. SVF plugs increased their percent expression of GS1 from an average of 29.08% and a standard deviation of 10.291% to an average of 53.346% with a standard deviation of 28.341%. Control plugs had 0% expression on day 7 and day 14 for both GS1 and αSMA expression. αSMA expression decreased from 12.5% with a standard deviation of 25.0% to 2.472% with a standard deviation of 4.472%

in EV plugs and went from 31.882% and a standard deviation of 22.405% to 30.727% and a standard deviation of 21.334% in SVF plugs. Day 14 cell numbers appear to be higher for SVF plugs with an average of 9.50 and standard deviation of 0.962, but values were not significant. One way ANOVA analysis returned the p-value for SVF plugs to be ~0.07 (α=0.05) when compared with the control group, which had an average of 0.167 and standard deviation of 0.236. EV plugs had an average of 0.867 cells on day 14 with a standard deviation of 1.386. The assessment of hydrogels *in-vitro* suggest GelMA synthesized at these conditions may not be best suited for cellular migration across tissue interfaces, and SVF gels may offer the best therapeutic benefit for angiogenesis given the already present cellular composition.

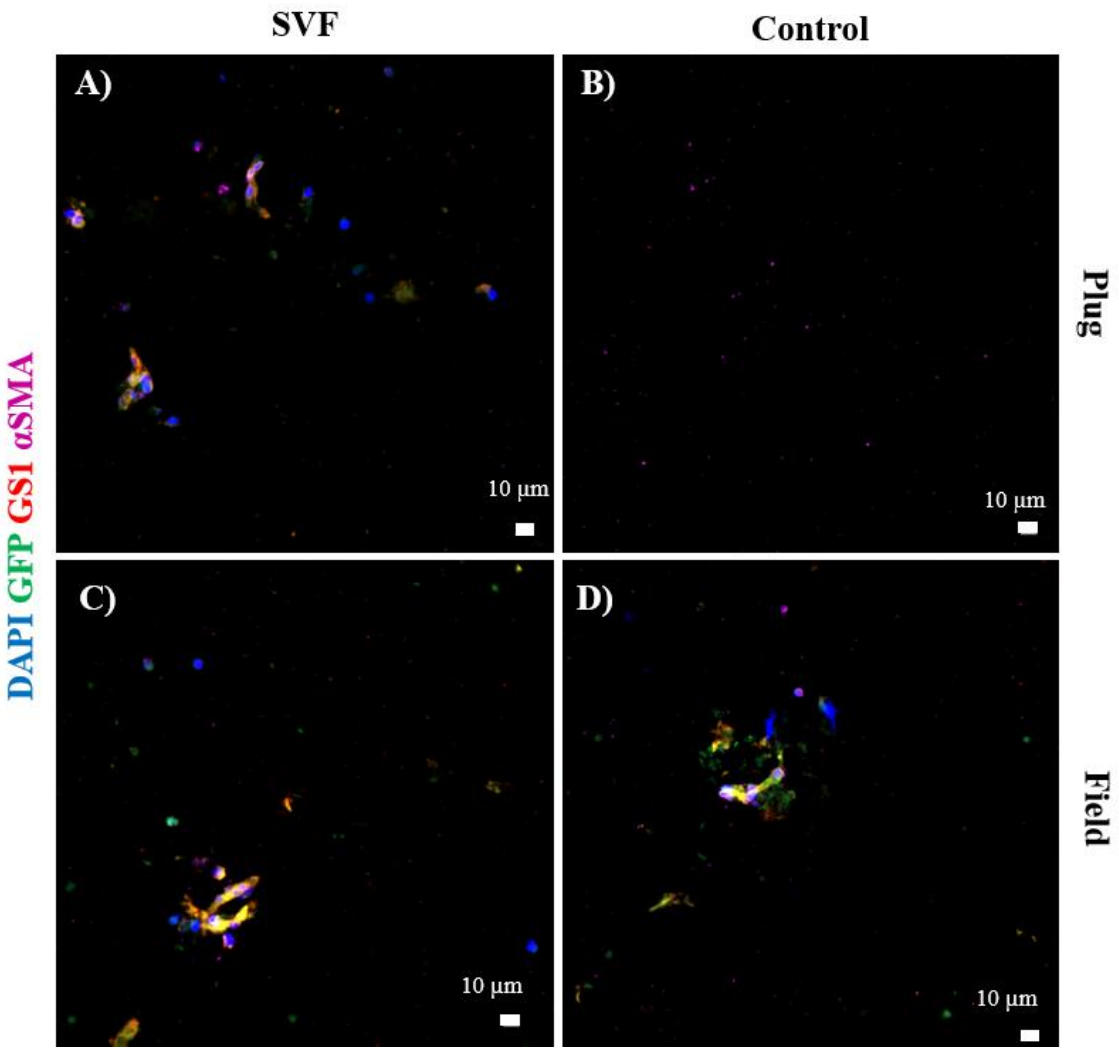

Figure 17: **Day 7 SVF plug-in-field images.** Day 7 plug-in-field 10X + Nyquist resolution images showing a A) SVF plug surrounded by its C) SVF cell field, and a B) blank control plug surrounded by its D) SVF cell field. Cells indicated by the DAPI stain fractionally express GS1-Rhodamine and αSMA. Scale bar 10 µm.

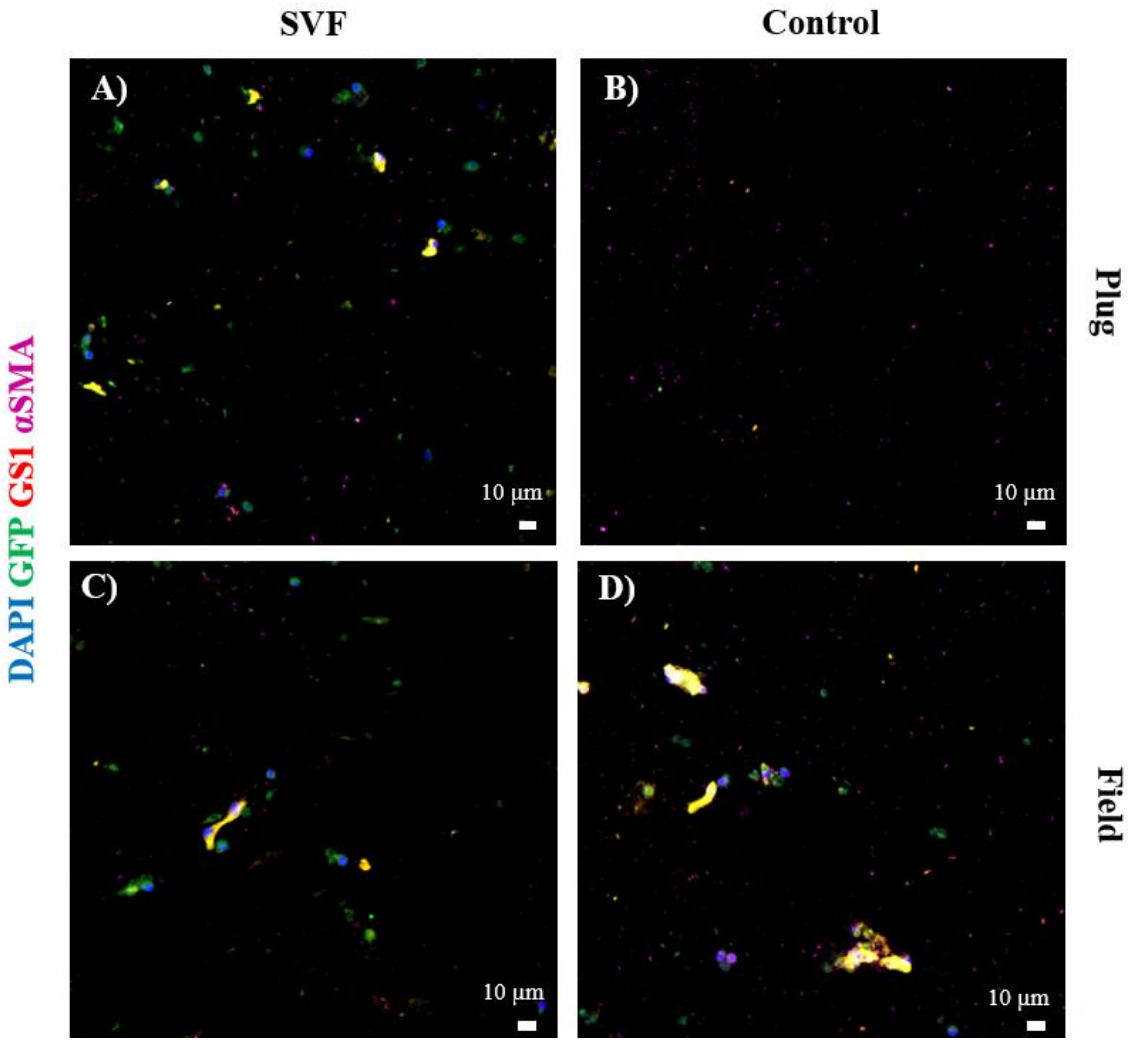

Figure 18: **Day 14 SVF plug-in-field images.** Day 14 plug-in-field 10X + Nyquist resolution images showing a A) SVF plug surrounded by its C) SVF cell field, and a B) blank control plug surrounded by its D) SVF cell field. Cells indicated by the DAPI stain fractionally express GS1-Rhodamine and αSMA. Scale bar 10 µm.

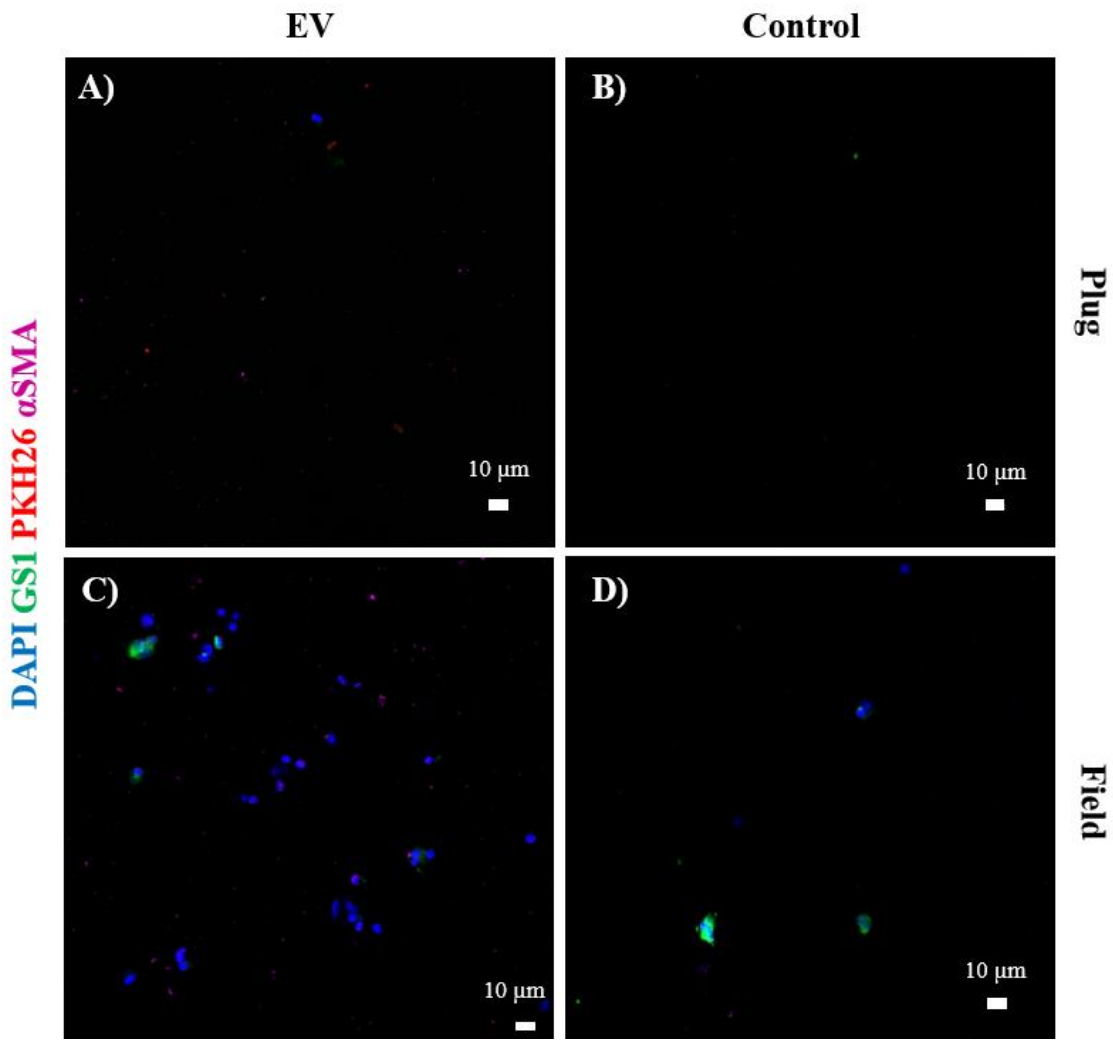

Figure 19: **Day 7 EV plug-in-field images.** Day 7 plug-in-field 10X + Nyquist resolution images showing a A) PKH26 labeled EV plug surrounded by its C) SVF cell field, and a B) blank control plug surrounded by its D) SVF cell field. Cells indicated by the DAPI stain fractionally express GS1 and αSMA. SVF cells from a non-GFP+ donor animal. Scale bar 10 µm.

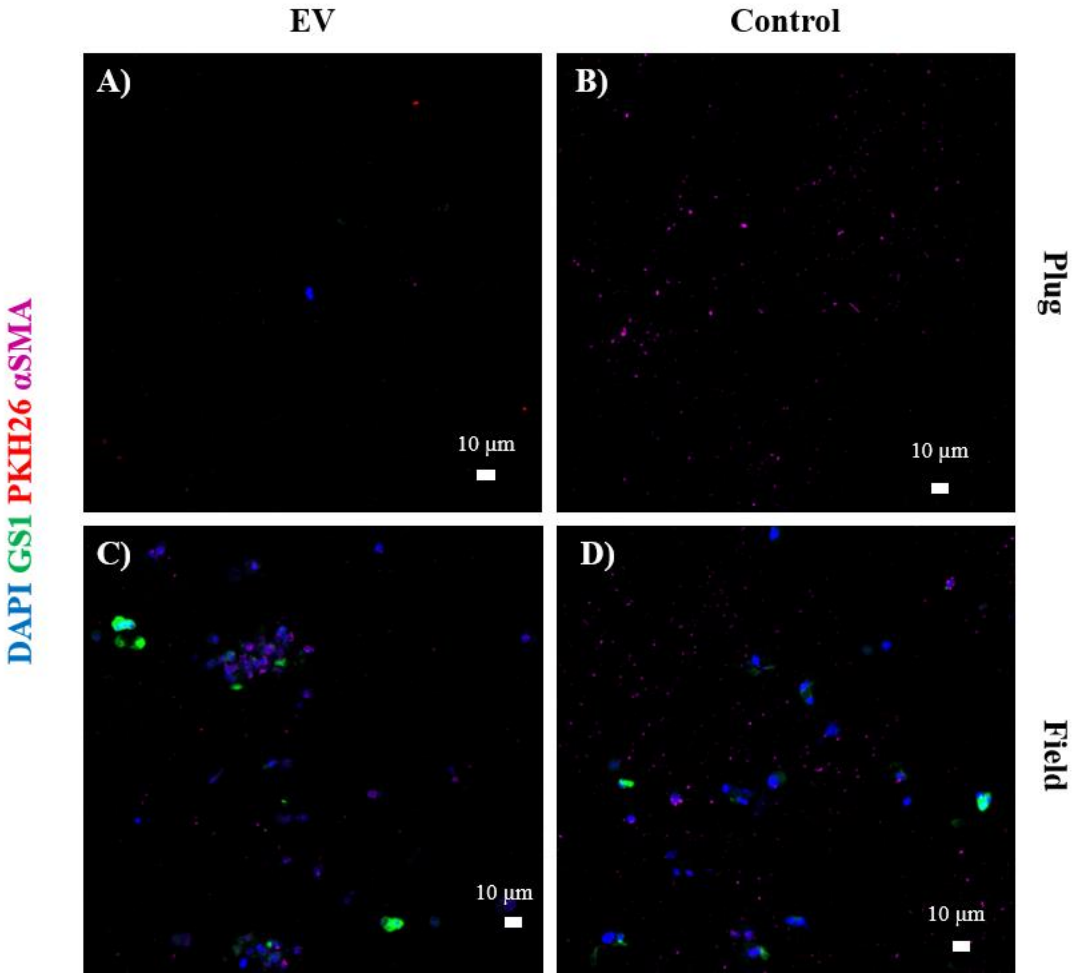

Figure 20: **Day 14 EV plug-in-field images.** Day 14 plug-in-field 10X + Nyquist resolution images showing a A) PKH26 labeled EV plug surrounded by its C) SVF cell field, and a B) blank control plug surrounded by its D) SVF cell field. Cells indicated by the DAPI stain fractionally express GS1 and αSMA. SVF cells from a non-GFP+ donor animal. Scale bar 10 µm.

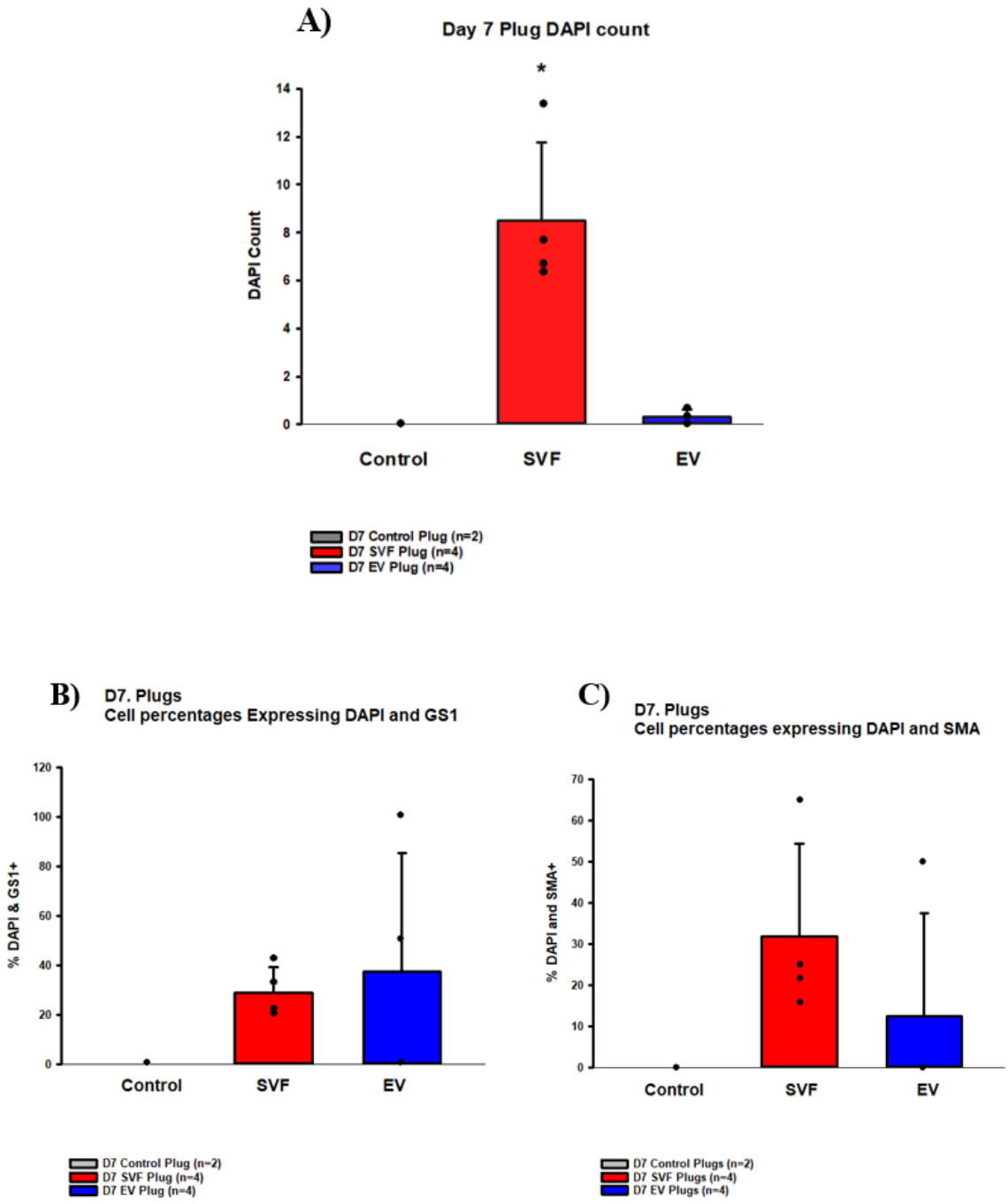

Figure 21: **Day 7 plug-in-field analysis.** Graphs representing day 7 average quantification of A) DAPI positive nuclei, and percent expression of cellular markers B) GS1 and C) αSMA across SVF, EV, and control plugs. DAPI positive cells of SVF plugs

differ significantly from the control A) with $p \leq 0.05$ (*). Percent expression of GS1 and αSMA did not differ significantly.

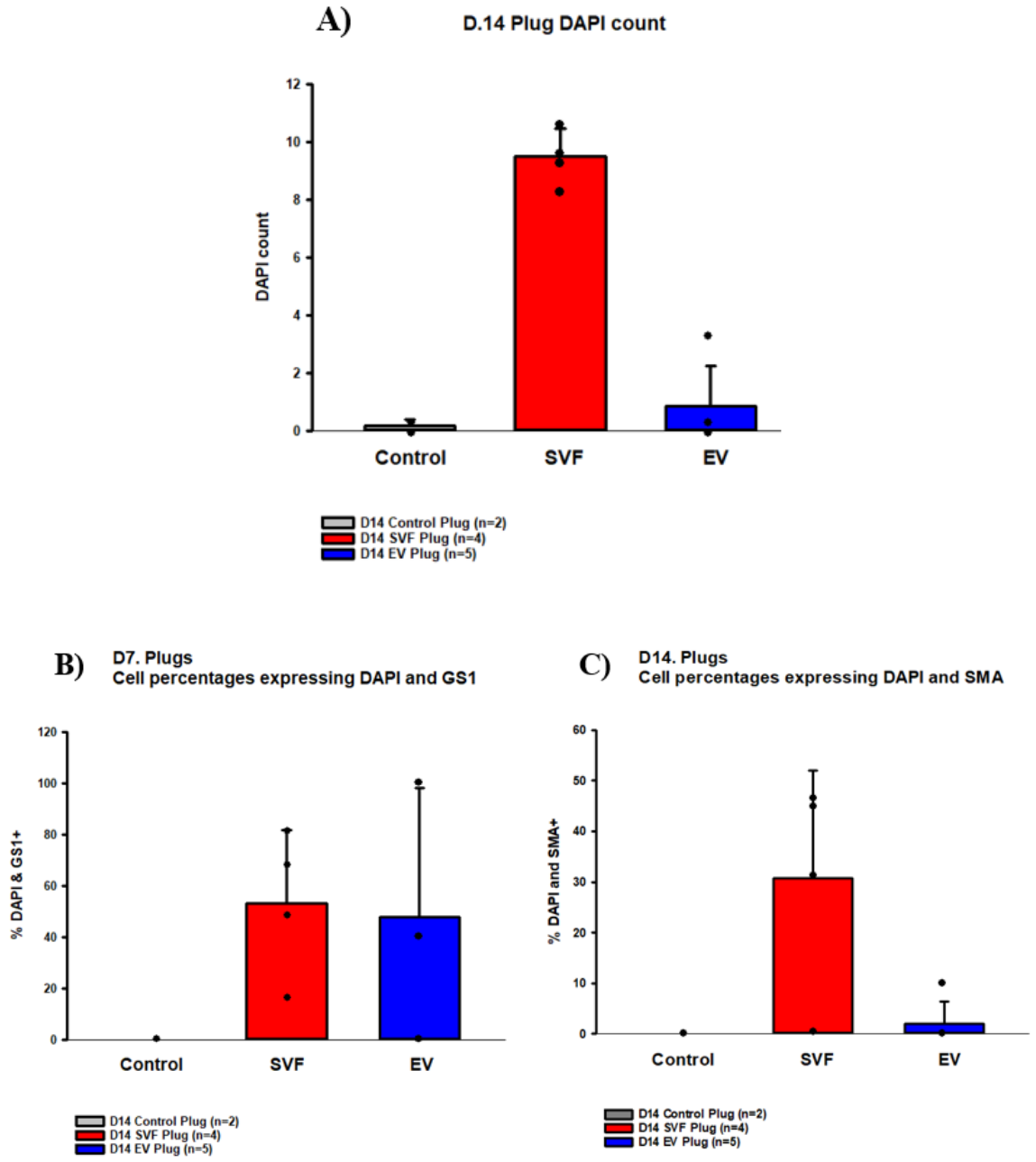

Figure 22: **Day 14 plug-in-field analysis.** Graphs representing day 14 average quantification of A) DAPI positive nuclei, as well as percent expression of cellular markers B) GS1 and C) αSMA across SVF, EV, and control plugs. Here neither the

DAPI cell count in plugs, GS1 percent expression, or αSMA percent expression differ significantly between groups.

in-vivo implantation of hydrogels:

The ability of the hydrogels to promote angiogenesis *in-vivo* was assessed by embedding hydrogels subcutaneously in Rag1 mice for two weeks. LDI was employed as a method to visualize subcutaneous blood flow upon explant and is represented in Figures 23 and 25 below. The black fur of the animals limited the capacity of laser doppler imaging to discern surface regions of blood flow in Rag1 mice and served as more of an observation, rather than quantitative assessment. Analysis of acquired histology images from different treatment groups after explant (Figure 27) was conducted by overlaying DAPI and Dextran filters to show perfused vasculature in ImageJ, where images were converted to binary and scaled to quantify percent vascular area. SVF hydrogels (Figure 24) displayed significantly higher percent vascular area compared to control groups via one way ANOVA (α=0.05). Differences between EV and control groups, as well as EV and SVF groups were not significant. Specifically, control gels had an average of 0.247% with a standard deviation of 0.679%, which was lower than EV gels that had an average 0.871% and a standard deviation of 0.926%. SVF gels had the highest percent vascularity per imaging field with an average of 10.980% with a standard deviation of 3.482%. Groups were also broken into male and female animals for similar analysis. Male SVF gels had an average of 13.015% vascularity with a standard deviation of 2.901%, which was significantly higher than EV gels (average: 1.370%, standard deviation: 1.528%) and control gels (average: 0.042%, standard deviation: 0.060%). Female SVF gels had an average 7.927% vascularity with a standard deviation of 0.762%, which was higher but not significantly different than EV gels (average: 0.538%, standard deviation: 0.363%) and control gels (average: 0.452%, standard deviation: 0.964). Furthermore, co-

expression of GFP+ signal and Dextran (Figure 24) stains suggest that it was the rat SVF cells incorporating into the perfused vasculature, rather than migration of vessels across tissue interfaces. Limited vascular presence was observed in EV and control gels as well, perhaps as a result of the of the gels' hinderance to migration of tissue across interfaces observed *in-vitro*.

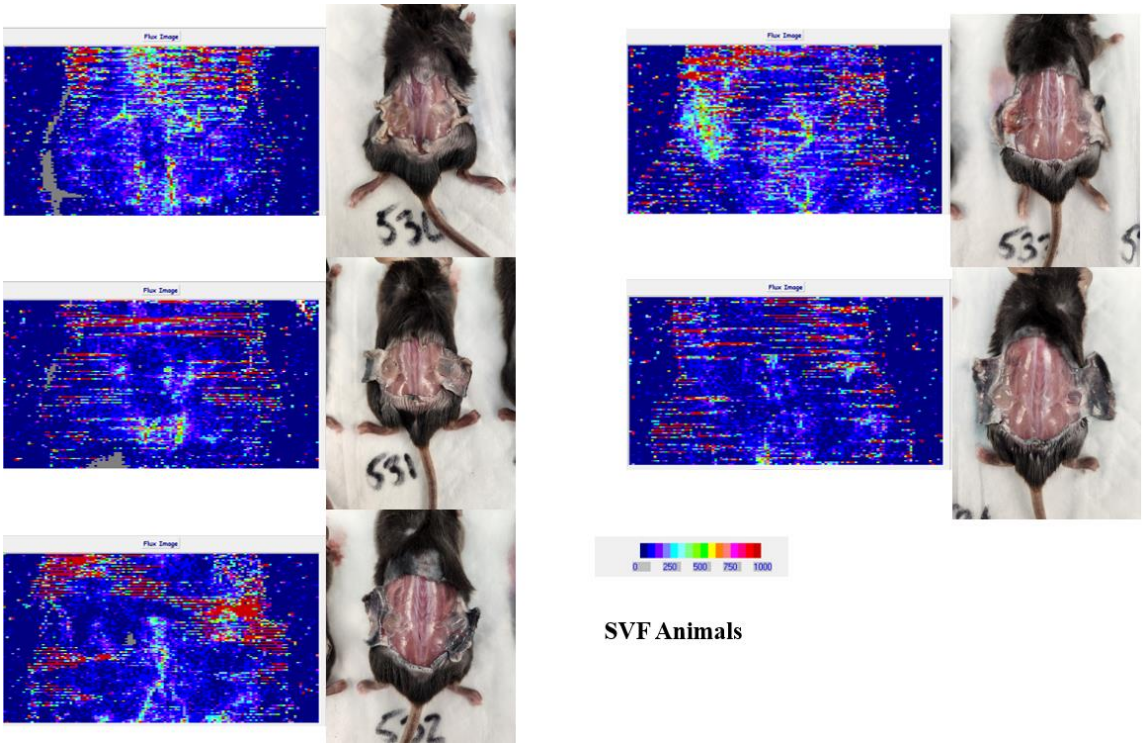

Figure 23: **Laser doppler imaging and gross anatomy images of SVF experimental animals.** LDI image results and gross anatomy images of gels prior to gel explant from animals receiving SVF gels on the left side and blank gels on the right. With blue indicating lower blood flow areas and red colors indicating areas of higher blood flow. Green and yellow areas indicate moderate blood flow levels.

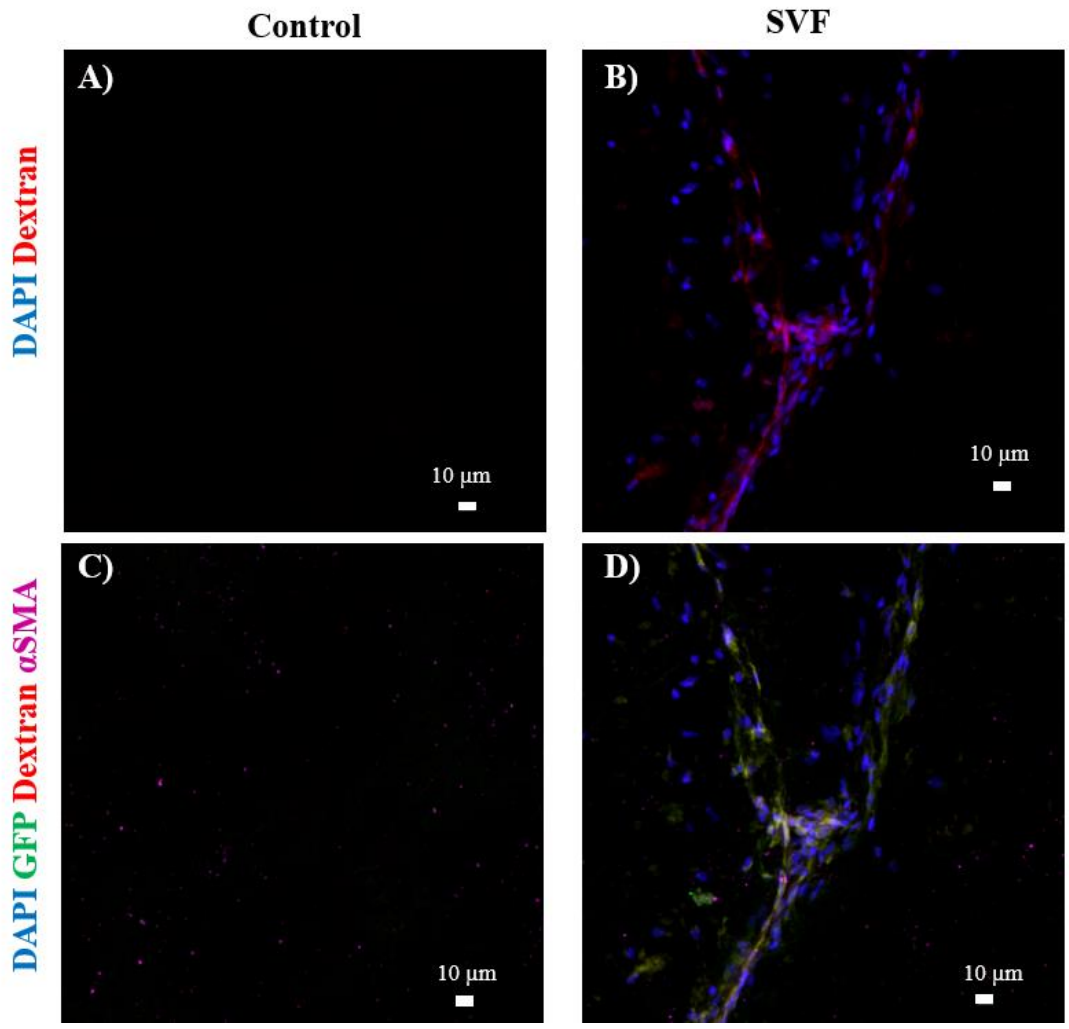

Figure 24: **Images of explanted SVF and control hydrogels.** Images of A) & C) control gels showing either A) DAPI-Dextran expression or C) DAPI, GFP, Dextran, and αSMA, where B) & D) show the same expression of the former in the SVF hydrogels. Scale bar 10 µm.

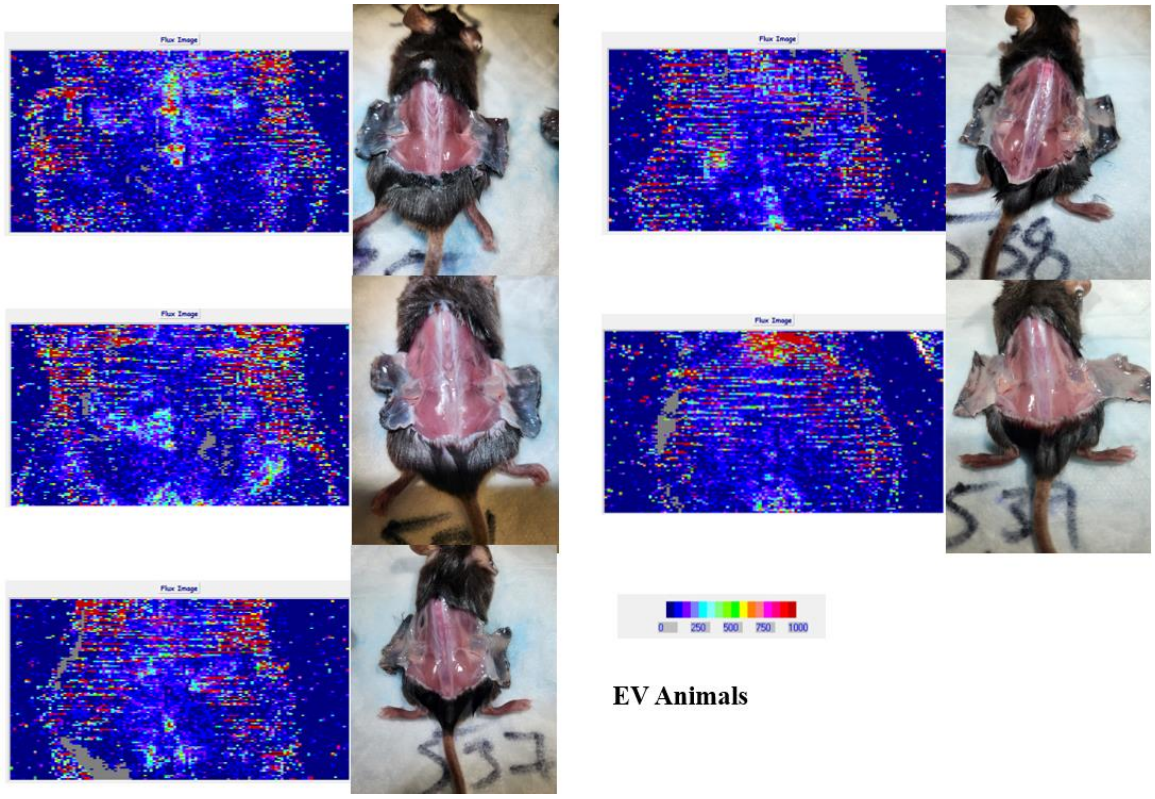

Figure 25: **Laser doppler imaging and gross anatomy images of EV experimental animals.** LDI image results and gross anatomy images of gels prior to gel explant from animals receiving EV gels on the left side and blank gels on the right. With blue indicating lower blood flow areas and red colors indicating areas of higher blood flow. Green and yellow areas indicate moderate blood flow levels.

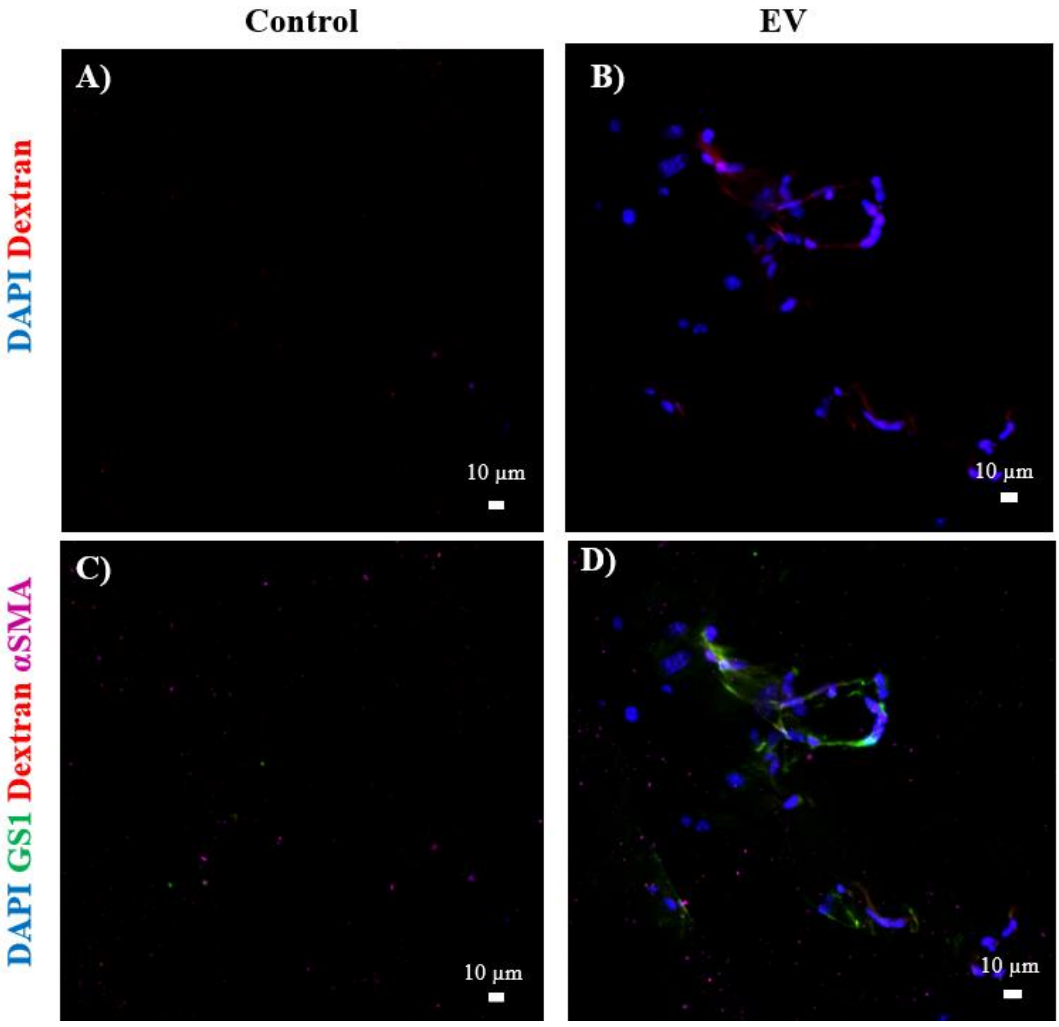

Figure 26: **Images of explanted EV and control hydrogels. I**mages of A) & C) control gels showing either A) DAPI-Dextran expression or C) DAPI, GS1, Dextran, and αSMA, where B) &D) show the same expression of the former in the EV hydrogels. Scale bar 10 µm.

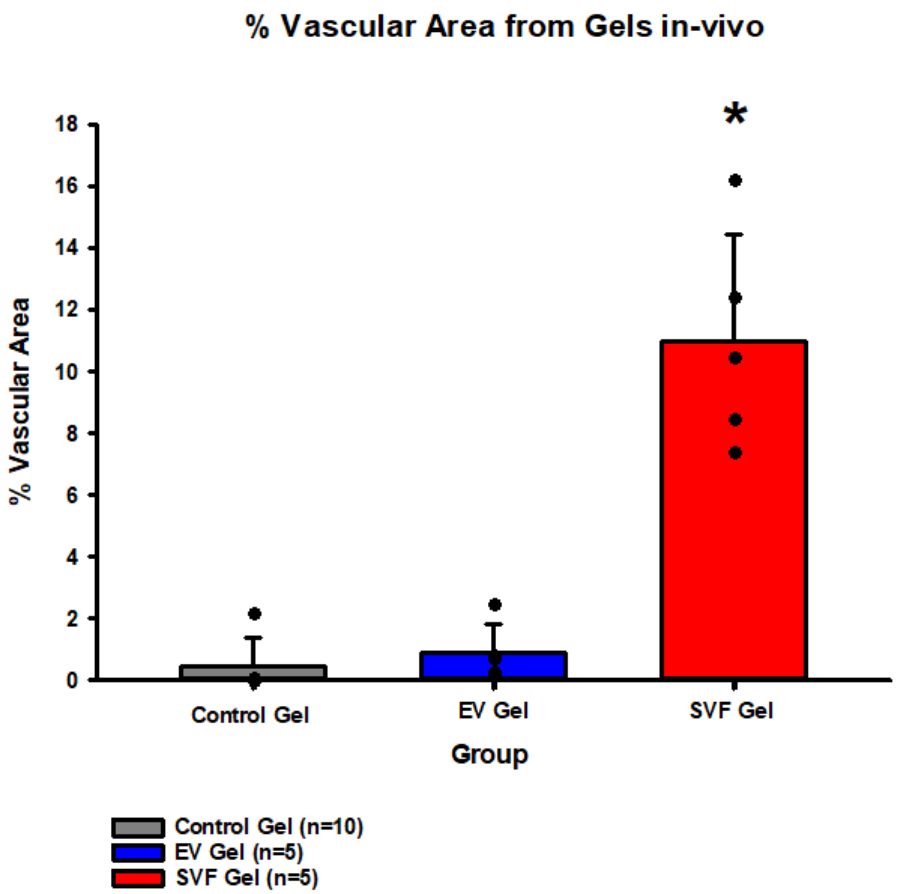

Figure 27: **Analysis of percent vascular area from explanted *in-vivo* gels.** Graph displaying average percent vascular area across experimental groups utilizing DAPI and Dextran staining. One way ANOVA (α=0.05) on ranks using Kruskal-Wallis and Dunn's method reveals the SVF hydrogels influence percent vascular area after 14 days significantly (*) when compared to the control group. Control gels had an average of 0.247% with a standard deviation of 0.679%, which was lower than EV gels that had an average 0.871% and a standard deviation of 0.926%. SVF gels had the highest percent vascularity per imaging field with an average of 10.980% with a standard deviation of 3.482%.

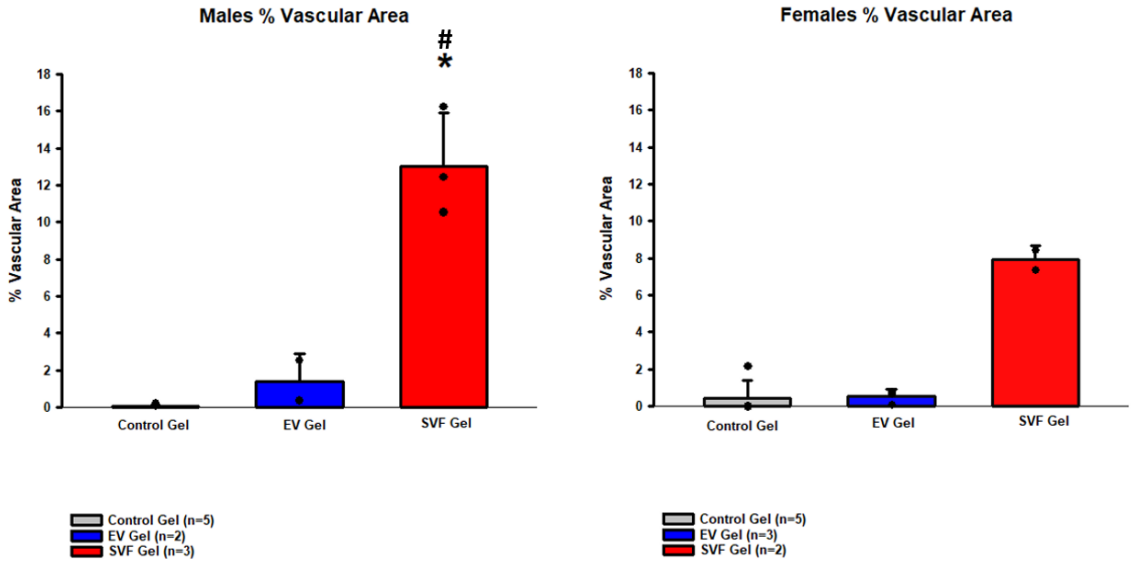

Figure 28: **Analysis of percent vascular area from explanted *in-vivo* gels, sex breakdown.** Graph displaying average percent vascular area across experimental groups utilizing DAPI and Dextran staining. One way ANOVA (α=0.05) pairwise comparison using the Holm-Sidak method. Male SVF gels had an average of 13.015% vascularity with a standard deviation of 2.901%, which was significantly higher than EV gels (average: 1.370%, standard deviation: 1.528%) and control gels (average: 0.042%, standard deviation: 0.060%). Female SVF gels had an average 7.927% vascularity with a standard deviation of 0.762%, which was higher but not significantly different than EV gels (average: 0.538%, standard deviation: 0.363%) and control gels (average: 0.452%, standard deviation: 0.964).

DISCUSSION

The major finding of this study is that SVF cells were more efficacious at promoting angiogenesis when compared to control gels, which were not significantly different than EV gels, *in-vivo*. Furthermore, based on the characterization of the hydrogels, GelMA proves a useful biomaterial for encapsulating, not only SVF, but also SVF derived EVs. GelMA was chosen as the biomaterial for this project because of high degree of biocompatibility [35], ability to be dual cross-linked [35], and tunable mechanical properties [32-34].

When originally designing the scaffold needed for experiments, a prolonged degradation was desired to give a stable structure for vessels to grow during incubation *in-vivo*. A prolonged release of SVF derived EVs was desired for better therapeutic benefit, which is why a dual cross-linked and higher percent gelatin scaffold was selected. However, results from release studies and plug-in-field experiments suggest the scaffold may require further optimization for angiogenesis applications.

Release experiments verified through both flow cytometry and microscopy that EV gels were not releasing SVF-derived EVs into the environment. This limits the conclusions that can be drawn from the EV therapies because the contents of the EVs need to be able to bind, signal, and integrate into host cells in order to elicit changes. The lack of EV release provides no cues to neighboring tissue to begin the process of angiogenesis.

Furthermore, plug-in-field experiments were used to assess the ability of EV gels to signal and induce changes across tissue interfaces. The lack of cellular presence observed in EV and control plugs suggest the gels may not have the ideal mechanics for cellular migration or tube formation. The rigidity of the matrix may have been too great for endothelial networks to mature.

Previously, lower percent hydrogels have demonstrated more rapid degradation [37], but softer mechanical characteristics [34]. Perhaps a lower percentage of gelatin would have given more ideal mechanics for angiogenesis [41]. While the degradation of GelMA is prolonged in this study, a lower percent gel and a single cross-linked matrix, as opposed to dual, may further improve the release of EVs from the gel. If a degradation could still be prolonged but achieve weight retention closer to ~20-40% of the gels initial weight, gels would be able to release more of their contents (EVs) as the biomaterial integrates and allow for easier migration of endothelial structures.

Nonetheless, even though the constructs did not promote tube formation *in-vitro*, gels did display perfused vascular networks *in-vivo*. SVF gels displayed significantly higher vascular area present in microscopy images compared control gels. This would indicate that regardless of gel mechanics or degradation, cellular gels may possess a greater therapeutic benefit than non-cellular gels. Expression of both GFP+ and Dextran signal from blood vessels in SVF constructs suggest the directed differentiation hypothesis may hold true for this model. The rat SVF cells themselves directly formed the blood vessels that gave SVF gels significantly higher vascular area. However, the lack of release of EVs from gels may insinuate that the EV gels didn’t get the chance to provide their therapeutic benefit and paracrine signal to the neighboring environment.

Absence of mature vessels *in-vitro* may also suggest cell culture conditions weren't optimized to induce spontaneous vessel formation. Previous studies using Matrigel, a softer material, and growth factor supplemented media SVF spontaneously formed tubes *in-vitro* at the same concentrations used for the gels in this study [38]. Atomic force microscopy has previously shown Matrigel to have an elastic modulus of ~440 Pa [42], where GelMA has shown a stiffness of 4-12 kPa in 10% single crosslinked gels [43], and rat tail collagen gels have shown to maintain a bulk stiffness of ~200 Pa while also possessing the ability to tune individual fiber strength beyond that without altering bulk material properties [44]. Plug-in-field experiments here used FBS and penicillin streptomycin supplemented media because of its use throughout other experiments, such as initial cell culture and EV detection experiments. Though tube formation did not occur, endothelial markers such as GS1 were expressed by cells during the plug-in-field experiments, in addition to smooth muscle actin expression. This expression combined with the high level of biocompatibility of the gels suggest that the gels possess the potential for spontaneous vessel formation but may require softer gel mechanics and growth factor supplemented media.

Furthermore, previous plug-in-field studies using collagen gels and micro-vessel fragments displayed the ability of fragments to branch and migrate from the plug into the field [39], which suggest migration through a biological gel may be easier with already established structures, rather than a single cell suspension which was used here.

FUTURE DIRECTIONS

This therapeutic can be further characterized moving forward. Limitations of the project timeline and its scope did not allow for full characterization of the hydrogel. To get a better idea of the gels inherit ability to promote angiogenesis, mechanical testing of the hydrogel should be done in compression and tension. Regardless of the mechanical testing results, the tunable mechanical properties of GelMA allow for adjustment of the scaffold makeup to be more suited for its application easily.

Furthermore, the gel could be imaged using scanning electron microscopy (SEM) to characterize the pore size of the gel. Quantifying the pore size of the gel may provide more insight into if the pores are ideal for angiogenesis and cellular/EV encapsulation. EVs could also be characterized further using transmission electron microscopy (TEM) to quantify the size of the particles that are loaded into gels and further confirm isolation of EV populations. The size of the EVs could also be compared with the pore size of the gel to determine ideal constructs for encapsulating and releasing EVs.

Additionally, experiments could be repeated using a lower percentage of gelatin to promote more degradation and release of contents for therapeutic benefit. Lower percentages of gelatin also suggest softer mechanical characteristics [34], which would allow for better blood vessel formation, albeit. Seeing that the gels encapsulated the EVs so well with minimal release, moving forward, only single crosslinked gels would most likely be needed.

After confirmation that EVs are being released from gels, more detailed release data should be gathered. Specifically, release studies should have more timepoints such as every other day out to a week to see prolonged diffusion of therapeutic EVs out of gels. Successful release could be further analyzed by applying a mathematical model to the release data to provide cues to the rate at which therapeutics are releasing and predict timepoints for maximum therapeutic benefit.

After adjusting the formulation of the hydrogels for better degradation and release, the plug-in-field experiment should be repeated using growth factor supplemented media in order to fully see the potential of these hydrogels at promoting spontaneous tube formation across tissue interfaces. Since SVF has shown spontaneous tube formation previously, this should be observed prior to repeating *in-vivo* experiments to really observe the most robust vascularization of non-cellular gels.

SUMMARY AND CONCLUSIONS

When directly observing the results of SVF and SVF derived EV hydrogels *in-vivo*, it becomes clear that there are benefits offered by cellular gels that are not possessed by non-cellular gels. Additionally, GelMA proves a useful biomaterial for encapsulation of SVF cells as well as nano sized EVs. GelMA also displayed a high level of biocompatibility with cell populations needed for tissue engineering applications. Furthermore, the biomaterial proves to have a prolonged degradation pattern at six and eight percent that can be used for many other tissue engineering applications, it is difficult to say which ones without further characterizing the gel. While GelMA can encapsulate EVs, its release of EVs remains limited based on the findings of this study, which further limits the therapeutic benefit of EV gels. However, the direct differentiation of cellular gels into mature perfused blood vessel networks that are not present in non-cellular gels may suggest stem cells are needed for maximum benefits in tissue engineered applications of angiogenesis.

REFERENCES

1. Kothawade, K. and C.N. Bairey Merz, *Microvascular coronary dysfunction in women: pathophysiology, diagnosis, and management.* Curr Probl Cardiol, 2011. **36**(8): p. 291-318.
2. Patel, H., et al., *Microvascular Disease and Small-Vessel Disease: The Nexus of Multiple Diseases of Women.* J Womens Health (Larchmt), 2020. **29**(6): p. 770-779.
3. Taqueti, V.R. and M.F. Di Carli, *Coronary Microvascular Disease Pathogenic Mechanisms and Therapeutic Options: JACC State-of-the-Art Review.* J Am Coll Cardiol, 2018. **72**(21): p. 2625-2641.
4. Bairey Merz, C.N., et al., *Treatment of coronary microvascular dysfunction.* Cardiovasc Res, 2020. **116**(4): p. 856-870.
5. Tracy, E., G. Rowe, and A.J. LeBlanc, *Cardiac tissue remodeling in healthy aging: the road to pathology.* Am J Physiol Cell Physiol, 2020. **319**(1): p. C166-C182.
6. Lloyd, P.G., H.T. Yang, and R.L. Terjung, *Arteriogenesis and angiogenesis in rat ischemic hindlimb: role of nitric oxide.* Am J Physiol Heart Circ Physiol, 2001. **281**(6): p. H2528-38.
7. Tracy, E.P., et al., *State of the field: cellular and exosomal therapeutic approaches in vascular regeneration.* Am J Physiol Heart Circ Physiol, 2022. **322**(4): p. H647-H680.
8. Kikuchi-Taura, A., et al., *Gap junction-mediated cell-cell interaction between transplanted mesenchymal stem cells and vascular endothelium in stroke.* Stem Cells, 2021. **39**(7): p. 904-912.
9. Kikuchi-Taura, A., et al., *Bone Marrow Mononuclear Cells Activate Angiogenesis via Gap Junction-Mediated Cell-Cell Interaction.* Stroke, 2020. **51**(4): p. 1279-1289.
10. Tang, J., et al., *Mesenchymal stem cells participate in angiogenesis and improve heart function in rat model of myocardial ischemia with reperfusion.* Eur J Cardiothorac Surg, 2006. **30**(2): p. 353-61.
11. Mikami, S., et al., *Autologous bone-marrow mesenchymal stem cell implantation and endothelial function in a rabbit ischemic limb model.* PLoS One, 2013. **8**(7): p. e67739.
12. Sharma, S., et al., *Randomized, Double-Blind, Placebo-Controlled Trial to Evaluate Safety and Therapeutic Efficacy of Angiogenesis Induced by Intraarterial Autologous Bone Marrow-Derived Stem Cells in Patients with Severe Peripheral Arterial Disease.* J Vasc Interv Radiol, 2021. **32**(2): p. 157-163.
13. Mathiasen, A.B., et al., *Autotransplantation of mesenchymal stromal cells from bone-marrow to heart in patients with severe stable coronary artery disease and refractory angina--final 3-year follow-up.* Int J Cardiol, 2013. **170**(2): p. 246-51.

14. Zhang, K., et al., *A nitric oxide-releasing hydrogel for enhancing the therapeutic effects of mesenchymal stem cell therapy for hindlimb ischemia.* Acta Biomater, 2020. **113**: p. 289-304.
15. Motawea, S.M., R.I. Noreldin, and Y.M. Naguib, *Potential therapeutic effects of endothelial cells trans-differentiated from Wharton's Jelly-derived mesenchymal stem cells on altered vascular functions in aged diabetic rat model.* Diabetol Metab Syndr, 2020. **12**: p. 40.
16. Gorjipour, F., et al., *Mesenchymal stem cells from human amniotic membrane differentiate into cardiomyocytes and endothelial-like cells without improving cardiac function after surgical administration in rat model of chronic heart failure.* J Cardiovasc Thorac Res, 2019. **11**(1): p. 35-42.
17. Ramakrishnan, V.M. and N.L. Boyd, *The Adipose Stromal Vascular Fraction as a Complex Cellular Source for Tissue Engineering Applications.* Tissue Eng Part B Rev, 2018. **24**(4): p. 289-299.
18. Bourin, P., et al., *Stromal cells from the adipose tissue-derived stromal vascular fraction and culture expanded adipose tissue-derived stromal/stem cells: a joint statement of the International Federation for Adipose Therapeutics and Science (IFATS) and the International Society for Cellular Therapy (ISCT).* Cytotherapy, 2013. **15**(6): p. 641-8.
19. Kamat, P., et al., *Adipose tissue and the vascularization of biomaterials: Stem cells, microvascular fragments and nanofat-a review.* Cytotherapy, 2020. **22**(8): p. 400-411.
20. Johnson, T.K., et al., *Exosomes derived from induced vascular progenitor cells promote angiogenesis in vitro and in an in vivo rat hindlimb ischemia model.* Am J Physiol Heart Circ Physiol, 2019. **317**(4): p. H765-H776.
21. Asahara, T., et al., *Bone marrow origin of endothelial progenitor cells responsible for postnatal vasculogenesis in physiological and pathological neovascularization.* Circ Res, 1999. **85**(3): p. 221-8.
22. Vittorio, O., et al., *Endothelial differentiation of mesenchymal stromal cells: when traditional biology meets mechanotransduction.* Integr Biol (Camb), 2013. **5**(2): p. 291-9.
23. Shi, R., et al., *Exosomes derived from mmu_circ_0000250-modified adipose-derived mesenchymal stem cells promote wound healing in diabetic mice by inducing miR-128-3p/SIRT1-mediated autophagy.* Am J Physiol Cell Physiol, 2020. **318**(5): p. C848-C856.
24. Xu, H., et al., *Exosomes derived from adipose tissue, bone marrow, and umbilical cord blood for cardioprotection after myocardial infarction.* J Cell Biochem, 2020. **121**(3): p. 2089-2102.
25. Wei, Y., et al., *MSC-derived sEVs enhance patency and inhibit calcification of synthetic vascular grafts by immunomodulation in a rat model of hyperlipidemia.* Biomaterials, 2019. **204**: p. 13-24.
26. Ge, Q., et al., *VEGF secreted by mesenchymal stem cells mediates the differentiation of endothelial progenitor cells into endothelial cells via paracrine mechanisms.* Mol Med Rep, 2018. **17**(1): p. 1667-1675.

27. Zhang, B., et al., *Co-culture of mesenchymal stem cells with umbilical vein endothelial cells under hypoxic condition.* J Huazhong Univ Sci Technolog Med Sci, 2012. **32**(2): p. 173-180.
28. Rowe, G., et al., *Stromal Vascular Fraction Reverses the Age-Related Impairment in Revascularization following Injury.* J Vasc Res, 2022: p. 1-15.
29. Rowe, G., et al., *Cell therapy rescues aging-induced beta-1 adrenergic receptor and GRK2 dysfunction in the coronary microcirculation.* Geroscience, 2022. **44**(1): p. 329-348.
30. Tracy, E.P., et al., *Stromal Vascular Fraction Restores Vasodilatory Function by Reducing Oxidative Stress in Aging-Induced Coronary Microvascular Disease.* Antioxid Redox Signal, 2022.
31. Zhao, D., et al., *GelMA combined with sustained release of HUVECs derived exosomes for promoting cutaneous wound healing and facilitating skin regeneration.* J Mol Histol, 2020. **51**(3): p. 251-263.
32. Sun, M., et al., *Synthesis and Properties of Gelatin Methacryloyl (GelMA) Hydrogels and Their Recent Applications in Load-Bearing Tissue.* Polymers (Basel), 2018. **10**(11).
33. Kim, P., et al., *Fabrication of poly(ethylene glycol): gelatin methacrylate composite nanostructures with tunable stiffness and degradation for vascular tissue engineering.* Biofabrication, 2014. **6**(2): p. 024112.
34. Shie, M.Y., et al., *Effects of Gelatin Methacrylate Bio-ink Concentration on Mechano-Physical Properties and Human Dermal Fibroblast Behavior.* Polymers (Basel), 2020. **12**(9).
35. Basara, G., X. Yue, and P. Zorlutuna, *Dual Crosslinked Gelatin Methacryloyl Hydrogels for Photolithography and 3D Printing.* Gels, 2019. **5**(3).
36. Council, N.R., *Guide for the Care and Use of Laboratory Animals: Eighth Edition*. 2011, Washington, DC: The National Academies Press. 246.
37. Yang, G., et al., *Enzymatically crosslinked gelatin hydrogel promotes the proliferation of adipose tissue-derived stromal cells.* PeerJ, 2016. **4**: p. e2497.
38. Maijub, J.G., et al., *Concentration-Dependent Vascularization of Adipose Stromal Vascular Fraction Cells.* Cell Transplant, 2015. **24**(10): p. 2029-39.
39. Strobel, H.A., et al., *Stromal Cells Promote Neovascular Invasion Across Tissue Interfaces.* Front Physiol, 2020. **11**: p. 1026.
40. Nichol, J.W., et al., *Cell-laden microengineered gelatin methacrylate hydrogels.* Biomaterials, 2010. **31**(21): p. 5536-44.
41. Nasser, M., et al., *Engineering microenvironments towards harnessing pro-angiogenic potential of mesenchymal stem cells.* Mater Sci Eng C Mater Biol Appl, 2019. **102**: p. 75-84.
42. Soofi, S.S., et al., *The elastic modulus of Matrigel as determined by atomic force microscopy.* J Struct Biol, 2009. **167**(3): p. 216-9.
43. Kim, C., et al., *Stem Cell Mechanosensation on Gelatin Methacryloyl (GelMA) Stiffness Gradient Hydrogels.* Ann Biomed Eng, 2020. **48**(2): p. 893-902.
44. Xie, J., et al., *Collagen Gels with Different Fibrillar Microarchitectures Elicit Different Cellular Responses.* ACS Appl Mater Interfaces, 2017. **9**(23): p. 19630-19637.

APPENDIX

Appendix A: non-Linear Regression Output of 6% GelMA Degradation by SigmaPlot

Nonlinear Regression **Monday, July 11, 2022 11:33:10 AM**

Data Source: Data 1 in Degradation Data
Equation: Exponential Decay, Single, 2 Parameter
f = a*exp(-b*x)

R	Rsqr	Adj Rsqr	Standard Error of Estimate
0.4806	0.2310	0.2062	8.1741

	Coefficient	Std. Error	t	P
a	84.8996	2.7649	30.7065	<0.0001
b	0.0030	0.0010	3.1414	0.0037

Analysis of Variance:

	DF	SS	MS
Regression	2	199498.5373	99749.2687
Residual	31	2071.2828	66.8156
Total	33	201569.8201	6108.1764

Corrected for the mean of the observations:

	DF	SS	MS
Regression	1	622.2416	622.2416
Residual	31	2071.2828	66.8156
Total	32	2693.5244	84.1726

95% Confidence:

Row	Predicted	95% Conf-L	95% Conf-U	95% Pred-L	95% Pred-U
1	84.8996	79.2606	90.5386	67.3005	102.4986
2	83.3639	78.6115	88.1162	66.0286	100.6992
3	81.8560	77.8719	85.8401	64.7154	98.9966
4	80.3753	76.9948	83.7559	63.3649	97.3858
5	78.9215	75.9163	81.9267	61.9817	95.8613
6	77.4939	74.5822	80.4056	60.5704	94.4174
7	76.0922	72.9972	79.1873	59.1362	93.0482
8	74.7158	71.2289	78.2028	57.6839	91.7478
9	73.3644	69.3577	77.3710	56.2185	90.5102
10	72.0373	67.4427	76.6319	54.7446	89.3300
11	70.7343	65.5199	75.9487	53.2667	88.2019
12	84.8996	79.2606	90.5386	67.3005	102.4986
13	83.3639	78.6115	88.1162	66.0286	100.6992
14	81.8560	77.8719	85.8401	64.7154	98.9966
15	80.3753	76.9948	83.7559	63.3649	97.3858

16	78.9215	75.9163	81.9267	61.9817	95.8613
17	77.4939	74.5822	80.4056	60.5704	94.4174
18	76.0922	72.9972	79.1873	59.1362	93.0482
19	74.7158	71.2289	78.2028	57.6839	91.7478
20	73.3644	69.3577	77.3710	56.2185	90.5102
21	72.0373	67.4427	76.6319	54.7446	89.3300
22	70.7343	65.5199	75.9487	53.2667	88.2019
23	84.8996	79.2606	90.5386	67.3005	102.4986
24	83.3639	78.6115	88.1162	66.0286	100.6992
25	81.8560	77.8719	85.8401	64.7154	98.9966
26	80.3753	76.9948	83.7559	63.3649	97.3858
27	78.9215	75.9163	81.9267	61.9817	95.8613
28	77.4939	74.5822	80.4056	60.5704	94.4174
29	76.0922	72.9972	79.1873	59.1362	93.0482
30	74.7158	71.2289	78.2028	57.6839	91.7478
31	73.3644	69.3577	77.3710	56.2185	90.5102
32	72.0373	67.4427	76.6319	54.7446	89.3300
33	70.7343	65.5199	75.9487	53.2667	88.2019

Fit Equation Description:

```
[Variables]
x = {col(19),col(19),col(19)}
y = {col(20,1,size(col(19))),col(21,1,size(col(19))),col(22,1,size(col(19)))}
reciprocal_y = 1/abs(y)
reciprocal_ysquare = 1/y^2
reciprocal_x = 1/abs(x)
reciprocal_xsquare = 1/x^2
reciprocal_pred = 1/abs(f)
reciprocal_predsqr = 1/f^2
weight_Cauchy = 1/(1+4*(y-f)^2)
'Automatic Initial Parameter Estimate Functions
F(q) = if(size(x)>1, if(total(abs(y))>0, ape(x,log(abs(y)),1,0,1), -306), 0)
asign(q) = if(mean(q)>=0,1,-1)
[Parameters]
a = if(F(0)[1]< 307, if(F(0)[1]>-307, asign(y)*10^F(0)[1], asign(y)*10^(-307)), asign(y)*10^307) "Auto
{{previous: 84.8996}} {{MinRange: -3}} {{MaxRange: 9}}
b = if(x50(x,y)-min(x)=0, 1,  -ln(.5)/(x50(x,y)-min(x)))  "Auto {{previous: 0.00304231}} {{MinRange:
0}} {{MaxRange: 1}}
[Equation]
f = a*exp(-b*x)
fit f to y
"fit f to y with weight reciprocal_y
"fit f to y with weight reciprocal_ysquare
"fit f to y with weight reciprocal_x
"fit f to y with weight reciprocal_xsquare
"fit f to y with weight reciprocal_pred
"fit f to y with weight reciprocal_predsqr
"fit f to y with weight weight_Cauchy
[Constraints]
b>0
[Options]
tolerance=01e-10
stepsize=1
iterations=200

Number of Iterations Performed = 8
```

Appendix B: non-Linear Regression of 8% GelMA Degradation by SigmaPlot

Nonlinear Regression **Monday, July 11, 2022 11:34:03 AM**

Data Source: Data 1 in Degradation Data
Equation: Exponential Decay, Single, 2 Parameter
f = a*exp(-b*x)

R	Rsqr	Adj Rsqr	Standard Error of Estimate
0.4334	0.1878	0.1616	9.7990

	Coefficient	Std. Error	t	P
a	88.2277	3.3154	26.6112	<0.0001
b	0.0031	0.0011	2.7418	0.0101

Analysis of Variance:

	DF	SS	MS
Regression	2	215171.1971	107585.5986
Residual	31	2976.6573	96.0212
Total	33	218147.8545	6610.5410

Corrected for the mean of the observations:

	DF	SS	MS
Regression	1	688.4632	688.4632
Residual	31	2976.6573	96.0212
Total	32	3665.1205	114.5350

95% Confidence:

Row	Predicted	95% Conf-L	95% Conf-U	95% Pred-L	95% Pred-U
1	88.2277	81.4658	94.9895	67.1295	109.3259
2	86.6199	80.9222	92.3175	65.8383	107.4015
3	85.0413	80.2654	89.8173	64.4933	105.5894
4	83.4916	79.4395	87.5437	63.0997	103.8835
5	81.9701	78.3678	85.5724	61.6628	102.2774
6	80.4763	76.9856	83.9670	60.1885	100.7642
7	79.0098	75.2989	82.7206	58.6829	99.3366
8	77.5699	73.3893	81.7506	57.1521	97.9878
9	76.1563	71.3532	80.9595	55.6020	96.7107
10	74.7685	69.2614	80.2757	54.0383	95.4987
11	73.4060	67.1570	79.6550	52.4665	94.3454
12	88.2277	81.4658	94.9895	67.1295	109.3259
13	86.6199	80.9222	92.3175	65.8383	107.4015
14	85.0413	80.2654	89.8173	64.4933	105.5894
15	83.4916	79.4395	87.5437	63.0997	103.8835
16	81.9701	78.3678	85.5724	61.6628	102.2774
17	80.4763	76.9856	83.9670	60.1885	100.7642
18	79.0098	75.2989	82.7206	58.6829	99.3366
19	77.5699	73.3893	81.7506	57.1521	97.9878
20	76.1563	71.3532	80.9595	55.6020	96.7107
21	74.7685	69.2614	80.2757	54.0383	95.4987
22	73.4060	67.1570	79.6550	52.4665	94.3454
23	88.2277	81.4658	94.9895	67.1295	109.3259

24	86.6199	80.9222	92.3175	65.8383	107.4015
25	85.0413	80.2654	89.8173	64.4933	105.5894
26	83.4916	79.4395	87.5437	63.0997	103.8835
27	81.9701	78.3678	85.5724	61.6628	102.2774
28	80.4763	76.9856	83.9670	60.1885	100.7642
29	79.0098	75.2989	82.7206	58.6829	99.3366
30	77.5699	73.3893	81.7506	57.1521	97.9878
31	76.1563	71.3532	80.9595	55.6020	96.7107
32	74.7685	69.2614	80.2757	54.0383	95.4987
33	73.4060	67.1570	79.6550	52.4665	94.3454

Fit Equation Description:

```
[Variables]
x = {col(19),col(19),col(19)}
y = {col(23,1,size(col(19))),col(24,1,size(col(19))),col(25,1,size(col(19)))}
reciprocal_y = 1/abs(y)
reciprocal_ysquare = 1/y^2
reciprocal_x = 1/abs(x)
reciprocal_xsquare = 1/x^2
reciprocal_pred = 1/abs(f)
reciprocal_predsqr = 1/f^2
weight_Cauchy = 1/(1+4*(y-f)^2)
'Automatic Initial Parameter Estimate Functions
F(q) = if(size(x)>1, if(total(abs(y))>0, ape(x,log(abs(y)),1,0,1), -306), 0)
asign(q) = if(mean(q)>=0,1,-1)
[Parameters]
a = if(F(0)[1]< 307, if(F(0)[1]>-307, asign(y)*10^F(0)[1], asign(y)*10^(-307)), asign(y)*10^307) "Auto
{{previous: 88.2277}} {{MinRange: -3}} {{MaxRange: 9}}
b = if(x50(x,y)-min(x)=0, 1,  -ln(.5)/(x50(x,y)-min(x))) "Auto {{previous: 0.00306525}} {{MinRange:
0}} {{MaxRange: 1}}
[Equation]
f = a*exp(-b*x)
fit f to y
'fit f to y with weight reciprocal_y
'fit f to y with weight reciprocal_ysquare
'fit f to y with weight reciprocal_x
'fit f to y with weight reciprocal_xsquare
'fit f to y with weight reciprocal_pred
'fit f to y with weight reciprocal_predsqr
'fit f to y with weight weight_Cauchy
[Constraints]
b>0
[Options]
tolerance=01e-10
stepsize=1
iterations=200

Number of Iterations Performed = 8
```

Appendix C: Descriptive Statistics Output by SigmaPlot for Viability Counts

Descriptive Statistics: Wednesday, December 7, 2022 11:05:45 AM

Data source: Data 1 in Viability Data

Column	Size	Missing	Mean	Std Dev	Std. Error	C.I. of Mean
Day 0	6	0	98.401	1.812	0.740	1.901
Day 1	6	0	99.383	1.512	0.617	1.587
Cells	12	0	98.958	3.608	1.042	2.293

Column	Range	Max	Min	Median	25%	75%
Day 0	4.000	100.000	96.000	98.718	96.727	100.000
Day 1	3.704	100.000	96.296	100.000	99.074	100.000
Cells	12.500	100.000	87.500	100.000	100.000	100.000

Column	Skewness	Kurtosis	K-S Dist.	K-S Prob.	SWilk W	SWilk Prob
Day 0	-0.273	-2.489	0.311	0.071	0.811	0.074
Day 1	-2.449	6.000	0.492	<0.001	0.496	<0.001
Cells	-3.464	12.000	0.530	<0.001	0.327	<0.001

Column	Sum	Sum of Squares
Day 0	590.406	58112.876
Day 1	596.296	59272.977
Cells	1187.500	117656.250

Appendix D: One-way ANOVA Output for Day 7 DAPI Plug Counts by SigmaPlot

One Way Analysis of Variance Friday, November 25, 2022 12:48:34 PM

Data source: Data 1 in invitro analysis

Normality Test (Shapiro-Wilk): Failed (P < 0.050)

Test execution ended by user request, ANOVA on Ranks begun

Kruskal-Wallis One Way Analysis of Variance on Ranks Friday, November 25, 2022 12:48:34 PM

Data source: Data 1 in invitro analysis

Group	N	Missing	Median	25%	75%
D7 SP DAPI	4	0	7.167	6.417	11.917
D7 EP DAPI	4	0	0.333	0.0833	0.583
D7 CP DAPI	2	0	0.000	0.000	0.000

H = 7.509 with 2 degrees of freedom. P(est.)= 0.023 P(exact)= 0.004

The differences in the median values among the treatment groups are greater than would be expected by chance; there is a statistically significant difference (P = 0.004)

To isolate the group or groups that differ from the others use a multiple comparison procedure.

All Pairwise Multiple Comparison Procedures (Dunn's Method) :

Comparison	Diff of Ranks	Q	P	P<0.050
D7 SP DAPI vs D7 CP DAPI	6.500	2.479	0.040	Yes
D7 SP DAPI vs D7 EP DAPI	4.250	1.985	0.141	No
D7 EP DAPI vs D7 CP DAPI	2.250	0.858	1.000	No

Note: The multiple comparisons on ranks do not include an adjustment for ties.

Appendix E: One-way ANOVA Output for Day 7 DAPI/GS1 Plug Expression by SigmaPlot

One Way Analysis of Variance Friday, November 25, 2022 12:58:00 PM

Data source: Data 1 in invitro analysis

Normality Test (Shapiro-Wilk): Passed (P = 0.163)

Equal Variance Test (Brown-Forsythe): Passed (P = 0.053)

Group Name	N	Missing	Mean	Std Dev	SEM
D7 SP DAPI/GS1	4	0	29.086	10.291	5.145
D7 EP DAPI/GS1	4	0	37.500	47.871	23.936
D7 CP DAPI/GS1	2	0	0.000	0.000	0.000

Source of Variation	DF	SS	MS	F	P
Between Groups	2	1915.071	957.535	0.932	0.438
Residual	7	7192.688	1027.527		
Total	9	9107.759			

The differences in the mean values among the treatment groups are not great enough to exclude the possibility that the difference is due to random sampling variability; there is not a statistically significant difference (P = 0.438).

Power of performed test with alpha = 0.050: 0.050

The power of the performed test (0.050) is below the desired power of 0.800.
Less than desired power indicates you are less likely to detect a difference when one actually exists.
Negative results should be interpreted cautiously.

Appendix F: One-way ANOVA Output for Day 7 DAPI/αSMA Plug Expression by SigmaPlot

One Way Analysis of Variance Wednesday, December 7, 2022 11:18:44 AM

Data source: Data 1 in invitro analysis

Normality Test (Shapiro-Wilk): Failed (P < 0.050)

Test execution ended by user request, ANOVA on Ranks begun

Kruskal-Wallis One Way Analysis of Variance on Ranks Wednesday, December 7, 2022 11:18:44 AM

Data source: Data 1 in invitro analysis

Group	N	Missing	Median	25%	75%
D7 SP DAPI/SMA	4	0	23.370	17.277	55.000
D7 EP DAPI/SMA	4	0	0.000	0.000	37.500
D7 CP DAPI/SMA	2	0	0.000	0.000	0.000

H = 4.562 with 2 degrees of freedom. P(est.)= 0.102 P(exact)= 0.142

The differences in the median values among the treatment groups are not great enough to exclude the possibility that the difference is due to random sampling variability; there is not a statistically significant difference (P = 0.142)

Appendix G: One-way ANOVA Output for Day 4 DAPI Plug Counts by SigmaPlot

One Way Analysis of Variance Friday, November 25, 2022 1:24:42 PM

Data source: Data 1 in invitro analysis

Normality Test (Shapiro-Wilk): Failed (P < 0.050)

Test execution ended by user request, ANOVA on Ranks begun

Kruskal-Wallis One Way Analysis of Variance on Ranks Friday, November 25, 2022 1:24:42 PM

Data source: Data 1 in invitro analysis

Group	N	Missing	Median	25%	75%
D14 SP DAPI	4	0	9.500	8.583	10.417
D14 EP DAPI	5	0	0.333	0.167	1.833
D14 CP DAPI	2	0	0.167	0.000	0.333

H = 7.636 with 2 degrees of freedom. P(est.)= 0.022 P(exact)= 0.009

The differences in the median values among the treatment groups are greater than would be expected by chance; there is a statistically significant difference (P = 0.009)

To isolate the group or groups that differ from the others use a multiple comparison procedure.

All Pairwise Multiple Comparison Procedures (Dunn's Method) :

Comparison	Diff of Ranks	Q	P	P<0.050
D14 SP DAPI vs D14 CP DAPI	6.500	2.263	0.071	No
D14 SP DAPI vs D14 EP DAPI	5.100	2.292	0.066	Do Not Test
D14 EP DAPI vs D14 CP DAPI	1.400	0.505	1.000	Do Not Test

Note: The multiple comparisons on ranks do not include an adjustment for ties.

Appendix H: One-way ANOVA Output for Day 14 DAPI/GS1 Plug Expression by SigmaPlot

One Way Analysis of Variance Friday, November 25, 2022 1:26:59 PM

Data source: Data 1 in invitro analysis

Normality Test (Shapiro-Wilk): Passed (P = 0.362)

Equal Variance Test (Brown-Forsythe): Failed (P < 0.050)

Test execution ended by user request, ANOVA on Ranks begun

Kruskal-Wallis One Way Analysis of Variance on Ranks Friday, November 25, 2022 1:26:59 PM

Data source: Data 1 in invitro analysis

Group	N	Missing	Median	25%	75%
D14 SP DAPI/GS1	4	0	58.067	24.069	77.902
D14 EP DAPI/GS1	5	0	40.000	0.000	100.000
D14 CP DAPI/GS1	2	0	0.000	0.000	0.000

H = 3.019 with 2 degrees of freedom. P(est.)= 0.221 P(exact)= 0.267

The differences in the median values among the treatment groups are not great enough to exclude the possibility that the difference is due to random sampling variability; there is not a statistically significant difference (P = 0.267)

Appendix I: One-way ANOVA Output for Day 14 DAPI/αSMA Plug Expression by SigmaPlot

One Way Analysis of Variance Friday, November 25, 2022 1:28:08 PM

Data source: Data 1 in invitro analysis

Normality Test (Shapiro-Wilk): Failed (P < 0.050)

Test execution ended by user request, ANOVA on Ranks begun

Kruskal-Wallis One Way Analysis of Variance on Ranks Friday, November 25, 2022 1:28:08 PM

Data source: Data 1 in invitro analysis

Group	N	Missing	Median	25%	75%
D14 SP DAPI/SMA	4	0	38.039	8.113	46.028
D14 EP DAPI/SMA	5	0	0.000	0.000	5.000
D14 CP DAPI/SMA	2	0	0.000	0.000	0.000

H = 7.303 with 2 degrees of freedom. P(est.)= 0.026 P(exact)= 0.023

The differences in the median values among the treatment groups are greater than would be expected by chance; there is a statistically significant difference (P = 0.023)

To isolate the group or groups that differ from the others use a multiple comparison procedure.

All Pairwise Multiple Comparison Procedures (Dunn's Method) :

Comparison	Diff of Ranks	Q	P	P<0.050
D14 SP DAPI/S vs D14 CP DAPI/S	5.750	2.002	0.136	No
D14 SP DAPI/S vs D14 EP DAPI/S	4.850	2.180	0.088	Do Not Test
D14 EP DAPI/S vs D14 CP DAPI/S	0.900	0.324	1.000	Do Not Test

Note: The multiple comparisons on ranks do not include an adjustment for ties.

Appendix J: One-way ANOVA on Percent Vascular Area from *in-vivo* Experiments

One Way Analysis of Variance Friday, December 2, 2022 1:50:49 PM

Data source: Data 1 in invivo analysis

Normality Test (Shapiro-Wilk): Failed (P < 0.050)

Test execution ended by user request, ANOVA on Ranks begun

Kruskal-Wallis One Way Analysis of Variance on Ranks Friday, December 2, 2022 1:50:49 PM

Data source: Data 1 in invivo analysis

Group	N	Missing	Median	25%	75%
EV Gel	5	0	0.689	0.207	1.626
SVF Gel	5	0	10.476	7.927	14.285
Control Gel	10	0	0.00667	0.000	0.0905

H = 14.250 with 2 degrees of freedom. (P = <0.001)

The differences in the median values among the treatment groups are greater than would be expected by chance; there is a statistically significant difference (P = <0.001)

To isolate the group or groups that differ from the others use a multiple comparison procedure.

All Pairwise Multiple Comparison Procedures (Dunn's Method) :

Comparison	Diff of Ranks	Q	P	P<0.050
SVF Gel vs Control Gel	12.000	3.703	<0.001	Yes
SVF Gel vs EV Gel	6.000	1.604	0.326	No
EV Gel vs Control Gel	6.000	1.852	0.192	No

Note: The multiple comparisons on ranks do not include an adjustment for ties.

Appendix K: One-way ANOVA on Percent Vascular Area from *in-vivo* Experiments (Males)

One Way Analysis of Variance Friday, December 2, 2022 1:51:31 PM

Data source: Data 1 in invivo analysis

Normality Test (Shapiro-Wilk): Passed (P = 0.194)

Equal Variance Test (Brown-Forsythe): Passed (P = 0.079)

Group Name	N	Missing	Mean	Std Dev	SEM
EV	2	0	1.370	1.528	1.081
SVF	3	0	13.015	2.901	1.675
male Ctl	5	0	0.0417	0.0604	0.0270

Source of Variation	DF	SS	MS	F	P
Between Groups	2	335.608	167.804	61.236	<0.001
Residual	7	19.182	2.740		
Total	9	354.790			

The differences in the mean values among the treatment groups are greater than would be expected by chance; there is a statistically significant difference (P = <0.001).

Power of performed test with alpha = 0.050: 1.000

All Pairwise Multiple Comparison Procedures (Holm-Sidak method):
Overall significance level = 0.05

Comparisons for factor:

Comparison	Diff of Means	t	P	P<0.050
SVF vs. male Ctl	12.974	10.732	<0.001	Yes
SVF vs. EV	11.645	7.706	<0.001	Yes
EV vs. male Ctl	1.328	0.959	0.369	No

Appendix L: One-way ANOVA on Percent Vascular Area from *in-vivo* Experiments (Females)

One Way Analysis of Variance Friday, December 2, 2022 1:52:48 PM

Data source: Data 1 in invivo analysis

Normality Test (Shapiro-Wilk): Failed (P < 0.050)

Test execution ended by user request, ANOVA on Ranks begun

Kruskal-Wallis One Way Analysis of Variance on Ranks Friday, December 2, 2022 1:52:48 PM

Data source: Data 1 in invivo analysis

Group	N	Missing	Median	25%	75%
EV	4	1	0.689	0.124	0.800
SVF	3	1	7.927	7.388	8.466
Female Ctrl	6	1	0.00833	0.00250	1.122

H = 5.542 with 2 degrees of freedom. P(est.)= 0.063 P(exact)= 0.041

The differences in the median values among the treatment groups are greater than would be expected by chance; there is a statistically significant difference (P = 0.041)

To isolate the group or groups that differ from the others use a multiple comparison procedure.

All Pairwise Multiple Comparison Procedures (Dunn's Method) :

Comparison	Diff of Ranks	Q	P	P<0.050
SVF vs Female Ctrl	5.900	2.329	0.060	No
SVF vs EV	3.500	1.266	0.616	Do Not Test
EV vs Female Ctrl	2.400	1.085	0.833	Do Not Test

Note: The multiple comparisons on ranks do not include an adjustment for ties.

CIRICULUM VITAE

Daniel Benson

Ph: (502) 693-7870

drbens02@louisville.edu

EDUCATION

2017-2021 B.S. in Bioengineering (Summa Cum Laude with honors), J.B. Speed School of Engineering, University of Louisville, Louisville, KY

2021-Present Master of Engineering, Thesis in Bioengineering, J.B. Speed School of Engineering, University of Louisville, Louisville, KY

Thesis: Establishing the Efficacy of Non-Cellular Components of Adipose-Derived Stromal Vascular Fraction in Promoting Angiogenesis

Commentors: Dr. Amanda Jo LeBlanc, PhD/Dr. Patricia Sara Arauz Soucy, PhD

EMPLOYMENT AND EXPERIENCE

2019 Student Co-Op Researcher for Dr. Anne K. Perl, PhD, Cincinnati Children's Hospital, Developmental Biology, Perinatal Institute, Cincinnati, OH

2021 *Bacterial Vaginosis Drug Delivery Capstone Project:* design and synthesize a multilayer phased drug delivery system that can encapsulate both drug and probiotics in a suppository to eliminate recurrence for Bacterial Vaginosis, while establishing quality assurance controls and performing appropriate risk analysis.

Mentor: Dr. Jill Steinbach-Rankins, PhD

2021 Research Assistant for Dr. William J. Zacharias, MD/PhD, Cincinnati Children's Hospital, Developmental Biology, Perinatal Institute, Cincinnati, OH

2021 *Rhesus Lung Injury Project:* Analysis of acquired histology images according to a lung-injury scoring system to assess the variance across the scores of different groups receiving inflammatory blockade treatment (publication three below).

Mentor: Dr. William J. Zacharias, MD/PhD

2021-Present Graduate student researcher for Dr. Amanda J. LeBlanc, PhD, Cardiovascular Innovation Institute and the Department of Physiology, Jewish Hospital and the University of Louisville, Louisville, KY

2021-2022 *Adipose-derived SVF Tissue Engineering Project:* design and synthesize SVF (Stromal Vascular Fraction) cell and exosome laden hydrogels that can be used as a therapy to re-vascularize ischemic tissues and to determine the efficacy of cell-free therapies (publication one below).

Mentors: Dr. Amanda Jo LeBlanc, PhD & Dr. Patricia Sara Arauz Soucy, PhD.

TECHNICAL ENGINEERING SKILLS

Bioinstrumentation- Data Acquisition
MATLAB
LabVIEW
SolidWorks
AutoCAD
Computational Modeling
Risk Analysis

TECHNICAL RESEARCH SKILLS

Animal Surgery
3D Organoid Cell Culture
Functional Histology
Microscopy
Pressure Myography
Flow Cytometry
Data Analysis

HONORS AND AWARDS

2017-2022 Kentucky Governor's Scholarship Recipient at the University of Louisville

2017-2021 Dean's List

2017-2021 Completion of the Honors program at the University of Louisville

2021 Summa Cum Laude Graduate (GPA > 3.9)

2022 Publication three below was chosen for front cover image of Science Translational Medicine

EXTRACURRICULAR ACTIVITIES

2017-2018 Active and Voting member of the J.B. Speed School Student Council at the University of Louisville

2017-2020 Member of the Biomedical Engineering Society at the University of Louisville

2018-2021 Member of Phi Delta Epsilon KY Beta chapter at the University of Louisville

COMMUNITY OUTREACH

2019 University of Louisville greenery initiative: members of Phi Delta Epsilon volunteered to landscape green spaces on campus and volunteered at the university's composting center.

2019 The Americana Center (Louisville, KY): members of Phi Delta Epsilon volunteered at the Americana Center to help organize a fun fall event for children of multi-cultural and refugee families in the Louisville area.

2019 Trivia Night Fundraiser: members of Phi Delta Epsilon organized and hosted a trivia night at the University of Louisville to raise money and awareness for Norton Children's Miracle Network.

PRESENTATIONS AND ABSTRACTS

1. **Benson D**, Beare J, Malovichko M, LeBlanc AJ. Research Louisville. Establishing the Efficacy of Non-Cellular Components of Adipose-Derived Stromal Vascular Fraction in Promoting Angiogenesis. 2022
2. Rowe G, Heng D.S, Beare JE, **Benson D**, LeBlanc AJ. North American Vascular Biology. Adipose-derived stromal vascular fractions rescue age-related impairment in angiogenesis within ex vivo mesenteric windows following injury. 2021

PUBLICATIONS

1. **Benson D**, Beare J, Malovichko M, LeBlanc AJ, Establishing the Efficacy of Non-Cellular Components of Adipose-Derived Stromal Vascular Fraction in Promoting Angiogenesis. In Preparation, expected submission Fall 2022.
2. Tracy EP, Stielberg V, Rowe G, **Benson D**, Nunes SS, Hoying JB, Murfee WL, LeBlanc AJ. State of the field: cellular and exosomal therapeutic approaches in vascular regeneration. Am J Physiol Heart Circ Physiol. 2022 Apr 1;322(4):H647-H680. doi: 10.1152/ajpheart.00674.2021. Epub 2022 Feb 18. PMID: 35179976; PMCID: PMC8957327.
3. Toth A, Steinmeyer S, Kannan P, Gray J, Jackson CM, Mukherjee S, Demmert M, Sheak JR, **Benson D**, Kitzmiller J, Wayman JA, Presicce P, Cates C, Rubin R, Chetal K, Du Y, Miao Y, Gu M, Guo M, Kalinichenko VV, Kallapur SG, Miraldi ER, Xu Y, Swarr D, Lewkowich I, Salomonis N, Miller L, Sucre JS, Whitsett JA, Chougnet CA, Jobe AH, Deshmukh H, Zacharias WJ. Inflammatory blockade prevents injury to the developing pulmonary gas exchange surface in preterm primates. Sci Transl Med. 2022 Mar 30;14(638):eabl8574. doi: 10.1126/scitranslmed.abl8574. Epub 2022 Mar 30. PMID: 35353543.